Journal of Field Robotics

WILEY

RESEARCH ARTICLE OPEN ACCESS

A Hybrid Parameters Estimation Approach for Power Consumption Modeling of Ground Mobile Robots With Unknown Payload

Parham Haji Ali Mohamadi[1,2] | Amin Khorasani[1,3] | Tom Verstraten[1,3] | Bram Vanderborght[1,2]

[1]Brubotics, Vrije Universiteit Brussel, Elsene, Brussels, Belgium | [2]IMEC, Heverlee, Leuven, Belgium | [3]Flanders Make, Heverlee, Leuven, Belgium

Correspondence: Parham Haji Ali Mohamadi (parham.haji.ali.mohamadi@vub.be)

Received: 25 March 2024 | **Revised:** 19 August 2024 | **Accepted:** 3 November 2024

Funding: The study was funded by the Interuniversitair Micro-Electronica Centrum VZW

Keywords: energy model | ground mobile robots | power consumption | robot energy losses

ABSTRACT

Typically, batteries are the main power source for mobile robots, and the practical constraints in carrying them pose challenges in achieving efficiency, autonomy, and safety objectives in robotic missions. Moreover, dealing with battery degradation requires a precise understanding of energy consumers' behavior in the system. Therefore, establishing an energy consumption model has an important role in addressing these challenges. This study focuses on the modeling and estimation of power consumption in indoor ground mobile robots with unknown payloads. We investigate key components and parameters that influence the actuation energy consumption of ground mobile robots equipped with DC motors, particularly in the context of pure rolling without slipping. To estimate the actuation power consumption of ground mobile robots, we present a hybrid parameters estimation approach. This method includes an offline step for estimating the mass-decoupled coefficients of a power model, followed by two online steps for estimating the robot's unknown payload and its actuation power consumption. Simulation and experimental results with a differential drive robot (Turtlebot3) validate the effectiveness of the proposed approach. Additionally, the performance of the proposed power consumption estimation method is compared with two other data-driven models based on multivariate linear regression and multilayer perceptron neural networks. The results demonstrate that the proposed method provides improved power consumption estimation accuracy on the selected indicators compared to the others. We also emphasize the importance of balancing the accuracy of power consumption estimation with its associated costs in the context of the proposed approach. This extra cost includes the energy needed for additional data measurement and processing. Considering this trade-off is crucial for the practical implementation and resource optimization in robotic systems.

1 | Introduction

The most distinctive feature of mobile robots compared to other robotic platforms is their ability to navigate in a given area while performing tasks in different contexts (Unger, Markert, and Müller 2018). These tasks may involve monitoring or manipulating a dynamic environment. The more complex these tasks become, the higher level of intelligence and autonomy needed for their safe and energy-efficient completion (Zhang, Zhang, and Yang 2020; Bozhinoski et al. 2019). In addition, batteries are the main choice for powering untethered robots (Verstraten et al. 2023). The limited power capacity of the batteries that a robot can carry is one of the challenges for achieving autonomy in its missions (Mikołajczyk et al. 2023). On the other hand, another set of challenges emerges due to battery aging and degradation, which limit its energy storage

and power output capabilities. Generally, operational conditions including overcharging, over-discharging, and high rates of charging and discharging affect battery life (Han et al. 2019). Therefore, it is necessary to optimize battery lifetime in accordance with the requirements of a robotic mission. Aiming for safety, energy efficiency, and autonomy goals while considering battery life requires knowing how the energy is consumed in the system. Thus, providing an accurate model for the energy consumption of mobile robots is beneficial across various aspects of robot design and operation, including estimation and prediction of robot mission energy consumption, energy-aware task scheduling and path planning, and designing an optimal controller for the robot (Touzout, Benazzouz, and Benmoussa 2022).

The analysis of previous studies (see Section 2) shows that most methods for estimating the energy consumption of ground mobile robots (GMRs) rely on dynamic modeling of the robots and their actuators or on physics-based external perspective modeling. Knowing the values of the parameters of these models, such as the motor's constant coefficients, gear ratios, transmission efficiency, the coefficient of friction between the wheel and the road surface, and the robot's mass and payload, even from the robot design stage, or estimating them using only prior data, cannot guarantee accurate estimation (Chikushi 2024). This is because the parameters may change over time, either in the long term or in the short term during a mission. On the other hand, data-driven methods, while capable of addressing some of these challenges, require continuous updating to maintain their accuracy. Particularly, when the robot's payload is unknown and varies during tasks, having an optimal approach to updating these models becomes crucial. There is a noticeable gap in research regarding the estimation and prediction of energy consumption in scenarios where the payload is variable and unknown.

The novel contribution of the present work is proposing a hybrid parameter estimation approach for power consumption modeling of a GMR with varying velocity profiles when the robot's unknown payload changes during task execution. Additionally, a detailed model of losses in GMRs equipped with DC motors is discussed to give an idea about the nature of the losses and the cause of their occurrence which can also be used in the optimal design of robots. The other aspect of the presented work is pointing out that in the context of the proposed method, the cost for enhancing the mass estimation and actuation power consumption estimation accuracy includes both the energy cost consumed for measuring and storing more data (keeping sensors on) and the computational costs to process that data over the additional time.

The presented work in the following sections focuses on estimating the actuation power while investigating the energy consumption in other subsystems of the robot. After reviewing the state of the art for GMRs power consumption in Section 2, in Sections 3–5 the methodology and proposed hybrid parameter estimation approach are discussed. We validated our approach through simulation and experiment in Sections 6 and 7, and the results are discussed in Section 8. Finally, we presented our conclusion from the research in Section 9.

2 | Related Works

Estimation and prediction methods are widely used in various applications and are developed for different data types. For example, when the predicted data belongs to the time series data category a long short-term memory (LSTM) prediction can be employed for long time series data sets to adapt to the changing trend of data sequences (Zhou et al. 2023) and some other classic prediction methods can be applied to other data types in this category such as oscillating time series (Wang et al. 2016), scaling time series (Dargie and Schill 2012), scheduling time series (Merkel, Stoess, and Bellosa 2010) and consolidation time series data (Srikantaiah, Kansal, and Zhao 2008).

In the case of mobile robots, several approaches exist for modeling their energy consumption. These methods can be categorized into three main sections. The first group of these methods relies on the dynamic model of the robot, the electromechanical equations of the robot's motors, or their combination. The other category contains models that analyze the robot's energy consumption from a physics-based external perspective, calculating it using kinetic energy and energy needed to overcome the traction resistance. The third group includes data-driven and machine-learning models which vary from linear regression models to more complex power consumption models using neural networks and other advanced techniques.

The dynamic model of a mobile robot can be used to relate the robot's state vector to the wheel's angular speed. When combined with the motors' electromechanical equations using circuit theory, the energy consumption model of the robot can be obtained. Kim and Kim (2012, 2017) used this method to propose an algorithm for generating a minimum-energy translational velocity trajectory for three-wheeled omni-directional mobile robots. Jaramillo-Morale et al. (2019) proposed an energy estimation model for differential drive mobile robots that uses the dynamic parameters of the robot and its motors for straight paths and they validated it along curved paths in Jaramillo-Morales et al. (2020) with variable accelerations and variable payloads. The results showed good accuracy for mission energy prediction along straight trajectories but in curved trajectories, the estimation error is up to 14%. Morales and Mendoza (2018) presented an energy consumption model for differential drive robots using kinematic and dynamic models of the robot and its motors but they just validated their model through a simulation and for a specific velocity and a known mass and assumed that power regeneration is allowed. Yacoub, Necsulescu, and Sasiadek (2013) integrated an energy consumption model of a differential drive robot that moves straight forward on a road with a predetermined road grade with different controllers and showed the capability of the model predictive control (MPC) to avoid torque saturation and decreasing the power consumption of the robot. Furthermore, Yao et al. (2024) used this approach to obtain the energy consumption model to improve the local path planning of the robot. they also assume that the robot's linear velocity and angular velocity are constants to simulate the predicted paths.

A conventional method for predicting the energy consumption of mobile robots relies on mathematical models that consider

the robot's physical characteristics and the environment in which it operates (Hou, Zhang, and Kim 2018). However, these models often have restrictions because they depend on certain assumptions made during their development, and they might not accurately represent the complexities of real-world situations. Moreover, as environmental conditions or the robot's state change over time, these models may become less reliable in their performance (Siwek et al. 2023). Wahab, Rios-Gutierrez, and El Shahat (2015) investigated energy loss components in a differential drive robot and presented techniques for experimental measurements of those losses and Mohammadpour et al. (2021) used these proposed techniques to analyze the effect of obstacle avoidance on robot's energy consumption. Moreover, Datouo et al. (2017) used the same techniques to develop an energy consumption model for optimizing the motion planning of a three-wheeled omnidirectional mobile robot. To show the importance of simulator-based power monitoring and estimation in solving different energy consumption-based problems, in Touzout, Benazzouz, and Benmoussa (2022) a mathematical energy model of a differential drive robot is integrated into the robot operating system (ROS) but authors neglected the electrical losses of motors in their work. Anjum, Khalid, and Manzoor (2024) further developed (Touzout, Benazzouz, and Benmoussa 2022) by integrating an advanced dynamic friction model (LuGre Friction Model) into their simulation framework. In a different approach from the other work in the literature, Kumar, Bensekrane, and Merzouki (2022) considered using a graphical and modular tool known as bond graph, to estimate the power consumption of a reconfigurable car-like structure robot with four steerable wheels. They used the model in the energy planning of the robot to complete a given task while neglecting the motors' losses. Sadrpour, Jin, and Ulsoy (2012, 2013b) compare a recursive least-squares estimation method based on the longitudinal dynamics model of an unmanned ground (UGV) with a Bayesian estimation with prior knowledge of the environment for predicting the mission energy of robot. They also investigated the relationship between power consumption and road grade and road surface condition in Sadrpour, Jin, and Ulsoy (2013a). Their result verified that the Bayesian estimation method can predict UGV energy consumption more accurately when prior knowledge of the environment is available. Quann et al. (2020) also proposed a method based on Gaussian process regression and the same longitudinal dynamics model to predict an off-road ground robot path energy cost. The model presented by Pentzer, Brennan, and Reichard (2022) to predict the energy used by a skid-steer drive robot is linear to three unknown parameters: resistance coefficient, a gain constant, and coefficient of friction. They used a recursive least squares (RLS) estimator to estimate the parameters during robot operation and refined the estimated model parameters using overhead imagery of the area of operation. The need for the overhead images which may not be available and valid after changes in the environment is one of the biggest challenges to use the proposed approach in this work. In another research, Effati, Skonieczny, and Balkcom (2023) adapted the same power model to compare the energy-optimal trajectories for a Husky UGV, which is also a skid-steer rover. Dogru and Marques (2018) investigated the effects of different parameters in a complex environment on the power consumption of a skid-steered robot and Hou et al. (2021) used the same method to propose a power model for a four-wheeled Mecanum robot. specifically, they studied the influences of road angle (upslope and downslope), temperature, and the change of the robot's center of gravity on its power consumption. Despite the relatively extensive investigation of the effective factors in the robot's energy consumption, the presented solutions in these works are still based on the assumption that all parameters, including the robot's payload, are known and static during the robotic mission.

On the other hand, some studies used data-driven and machine-learning approaches for the energy consumption modeling of mobile robots. In these studies, the power consumption of the GMRs under different conditions is measured and estimated using prior data and the trained numerical models (Chikushi 2024). Mei et al. (2005) studied the power consumption of the Pioneer 3*DX*, which is a two-wheeled differential drive robot. They applied a first-order linear regression model to motion power and robot velocity data, both in a straight line and along a circular path, to estimate the power consumption of the robot's motion. They suggest using the energy consumption model for dynamic power management of components and real-time scheduling of tasks in robotic missions. Jaiem et al. (2016, 2021) investigated the power consumption of the same Pioneer 3*DX* robot. They proposed an identification protocol to establish the energy consumption models for different configurations of the robot and highlighted the optimal velocity that minimizes motion energy. In both works a second-order polynomial regression model is used to estimate the motion power with respect to the robot's linear velocity but only the non-acceleration scenarios are assumed. Parasuraman et al. (2012) studied components of energy consumption in a small differential wheeled robot (Khepera *III*) and further presented a method for predicting the robot's energy requirements in Parasuraman et al. (2014) based on predetermined power models of the robot's components. This model can be utilized in online energy optimization to enhance the safety and reliability of robots in hostile environments. The assumption is made that the effect of acceleration is negligible in motion power consumption. Furthermore, they added the mass component to their proposed first-order linear regression equation to model the payload. Leng et al. (2024) simplified the physics-based power consumption equation of an electric vehicle to propose a data-driven power consumption estimation framework for AGVs. Using the multivariate linear regression method, they fit the collected data to the proposed model but did not consider variable payload conditions in their experiments. Liu et al. (2023) implemented three models (linear regression, polynomial regression, and multilayer perception) to predict motion energy consumption in a robot with four Mecanum wheels and used control commands and feedback from four motors to build the model. They also applied the energy prediction model to obstacle avoidance and guided energy-efficient path selection. Although the result showed a reduction in energy consumption compared to the baseline, the effects of the changing environment and the robot's parameters like the robot's payload are not taken into account in this research. Góra et al. (2021) compared a mathematical model with an artificial neural network model for energy consumption of differential derive robots and skid-steer drive robots. Their result showed that AI methods are more universal and can be used when there

is not sufficient knowledge of the kinematic structure of a robot. Sakayori and Ishigami (2021) constructed the power consumption model of a simulated planetary rover using the vehicle velocity, inclination of the slope, and the angle of attack as inputs of a feed-forward neural network with back-propagation algorithm in an on-slope traversal. In a recent study, Chikushi (2024) proposed a method for power consumption estimation of the drive system for a skid-steering type mobile robot in long-duration and long-distance in-door operations using a neural network model and considering commanded linear velocity, commanded angular velocity, and vibration (acceleration) in the X–Y–Z axis direction. In both these research, the rectified linear unit function is used as the activation function for the middle and output layers.

Despite the diverse methodologies in the literature, challenges for accurate power estimation of GMRs persist. Methods that consider the equations of the robot and its motors generally assume that the model parameters are known and fixed during the robotic mission. Additionally, assumptions such as ignoring friction or acceleration during operation make it difficult to apply these methods in complex environments. On the other hand, physics-based methods are used with more diverse robot types, and some studies employ various parameter estimation methods to determine model parameters. However, none of these studies investigate the effects of varying payloads during the robot's mission. Data-driven and machine-learning methods can account for complex energy consumption processes, such as complex interactions between the track or wheels, which might be challenging to address in theoretical models. Nevertheless, these methods may not be universally accurate across all operating conditions, as they are trained under specific scenarios (Licea, Ghogho, and Saska 2024). Overall, the requirement for accurate parameter knowledge of models, static or at least known payload assumptions, and a high degree of specificity to the type of GMRs, makes it difficult to use these methods in practice (see Table 1). In this paper, the proposed approach can be applied to GMRs equipped with DC motors in pure rolling without slipping.

3 | Methodology

In general, subsystems of a mobile robot can be categorized as power source and its battery management system, computing (including high-level embedded computers, low-level microcontrollers, and components for data storage and access), interception and/or exteroception sensing components, actuation for robot movement and interaction with the environment, and communication subsystems for interfacing with other robots, base stations, or controllers (Parasuraman et al. 2014) as illustrated in Figure 1. The energy consumption model of the robot is a function of these subsystems. Therefore, the general power model of a robot can be expressed as follows:

$$P = P_{sen} + P_{com} + P_{comm} + P_{act} \tag{1}$$

where P represents the robot instance power, and $P_{sen}, P_{com}, P_{comm}, P_{act}$ denote the instance power for sensing, computing, communication, and actuation, respectively. Under consistent operating conditions and configuration of GMRs, the components of instantaneous power consumption in Equation (1) are constant across various tasks, except for the actuation power consumption P_{act} which varies depending on the specific task. This assumption holds true based on our experimental validation and aligns with findings in related works (Liu et al. 2023; Touzout, Benazzouz, and Benmoussa 2022; Hou, Zhang, and Kim 2018; Góra et al. 2021). Further discussion on this matter will be provided in Section 7.

In this work, a hybrid parameter estimation method is employed to estimate the actuation instance power in the presence of an unknown payload during GMR task execution. The proposed approach is shown in Figure 2 and consists of the following three steps.

i. In the first step, mass-decoupled coefficients of the proposed actuation power consumption model will be estimated using an offline method. These coefficients are derived from a comprehensive physics-based prescriptive analysis of the GMRs power consumption and their estimation is considered as an optimization problem. This estimation step will be done using the projected gradient descent method and the necessary data, including measured velocity and power consumption, will be collected during the GMR's operation with different payloads (zero payload and full payload) and speeds.

ii. The second step involves online unknown payload estimation. In this step, the proposed power consumption model is reformulated as a quadratic equation with respect to the robot's total mass (including unknown payload). Based on the tasks' behavior in the operational condition, this step can be conducted periodically while the robot executes tasks or during a predetermined time interval at the beginning of each task. Moreover, a weighted average will be computed over the estimated mass to reduce the effects of invalid estimations while the robot is not moving or moves at low speeds.

iii. The third step is an online calculation of actuation power consumption using the estimated mass-decoupled coefficients from the first step and payload mass estimation in the second step. The limited floating point operations needed for this actuation power consumption calculation is one of the principle points of this step.

Furthermore, the actuation power model employed in this research breaks down the power consumption of the actuating system into its components, deducing the power losses and consumption of its various parts.

4 | Actuation Power Consumption Model

In ground-wheeled robots, the actuating power is mainly affected by payload, motors' losses, road grade, rolling friction, and robot velocity and acceleration profile (Zorbas and Razafindralambo 2015; Gürgöze and Türkoğlu 2022). Given the extensive use of GMRs in indoor warehouse settings (Góra et al. 2021), it is reasonable to assume that the rolling friction coefficient remains constant during the execution of various tasks. This assumption holds true if the

TABLE 1 | Overview of power consumption estimation approaches in GMRs.

Authors	Year	Specified rover type	VP[a]	UP[b]	Approach
					Dynamic model approach
Kim and Kim (2012, 2017)	2012, 2017	Three-wheeled omni-directional	No	No	Mixed known dynamics models of the robot and the DC motor
Jaramillo-Morales et al. (2019, 2020)	2019, 2020	Differential drive	Yes	No	Mixed known dynamics models of the robot and the DC motor
Morales and Mendoza (2018), Yacoub, Necsulescu, and Sasiadek (2013), Yao et al. (2024)	2018, 2013, 2024	Differential drive	No	No	Mixed known dynamics models of the robot and the DC motor
					Physics-based approach
Sadrpour, Jin, and Ulsoy (2012, 2013a, b)	2012, 2013, 2013	Skid-steer	No	No	Vehicle longitudinal dynamics model
Quann et al. (2020)	2020	Four-wheel drive	No	No	Vehicle longitudinal dynamics model and direct power model
Wahab, Rios-Gutierrez, and El Shahat (2015), Datouo et al. (2017), Touzout, Benazzouz, and Benmoussa (2022), Anjum, Khalid, and Manzoor (2024), Mohammadpour et al. (2021)	2015, 2017, 2022, 2024, 2021	Differential drive	No	No	Mathematical physics-based power model of robot and DC motor
Datouo et al. (2017)	2017	Three-wheeled omni-directional	No	No	Mathematical physics-based power model of robot and DC motor
Hou et al. (2021)	2021	four-wheeled mecanum wheel	No	No	Mathematical physics-based power model of robot and DC motor
Dogru and Marques (2018)	2018	Skid-steer	No	No	Mathematical physics-based power model of robot and DC motor
Pentzer, Brennan, and Reichard (2022)	2022	Skid-steer	No	No	First-order model of longitudinal and angular speeds with online estimation of ICR kinematics and terrain-related model parameters
Effati, Skonieczny, and Balkcom (2023)	2023	Skid-steer	No	No	First-order model of longitudinal and angular speeds with known ICR kinematics
Kumar, Bensekrane, and Merzouki (2022)	2022	reconfigurable	No	No	Physics-based and Power-based graphical modeling (bond graph)
					Data-driven and machine-learning approach
Mei et al. (2005)	2005	Differential drive	Yes	No	First-order linear regression model of longitudinal speed
Jaiem et al. (2016, 2021)	2016, 2021	Differential drive	No	No	Second-order polynomial regression model of longitudinal speed
Parasuraman et al. (2012, 2014)	2012, 2014	Differential drive	Yes	No	First-order linear regression model of longitudinal speed and mass
Leng et al. (2024)	2024	Ackermann steering wheeled	No	Yes	Multivariate linear regression model of longitudinal speed and angular velocity

(Continues)

TABLE 1 | (Continued)

Authors	Year	Specified rover type	VP[a]	UP[b]	Approach
Liu et al. (2023)	2023	four-wheeled mecanum wheel	No	Yes	Linear regression, polynomial regression, and multilayer perceptron (MLP) model of motos' control commands and their feedback
Góra et al. (2021)	2021	Differential drive and skid-steer	No	No	Neural networks model with linear and angular speeds, rolling friction, static friction, mass inputs
Sakayori and Ishigami (2021)	2021	Planetary rover	No	Yes	Feed-forward NN with back-propagation. Reference velocity, slope angle, and heading angle are set as the input layer.
Chikushi (2024)	2024	Skid-steer	No	Yes	NN with commanded linear and angular velocity, and vibration (acceleration as the input layer.
					Proposed aproach
Ours		Not specified	Yes	Yes	Hybrid parameters estimation for mathematical physics-based power model of robot and DC motor

[a]Variable payload.
[b]Unknown payload.

ground surface conditions remain constant throughout the entire warehouse. Although there are methods for detecting the surface change such as the one introduced in (Pentzer, Brennan, and Reichard 2022). Additionally, it is assumed that the road grade is equal to zero, which is a reasonable assumption for indoor use cases.

The power consumption model for the actuation mechanism of a GMR can be derived by breaking down the mechanism into four primary subsystems: drive, motor, gear, and robot dynamics. This power breakdown is shown in Figure 3. To obtain the actuation power consumption, the power losses and consumption of each subsystem are deducted from the source power.

4.1 | Drive Losses

Typically, datasheets provide a drive controller efficiency, denoted as η_c, in the range of 90%–95% (Verstraten 2018). The controller efficiency, η_c can be used to compute the power drawn from the power source, P_{source}, using the controller efficiency function $C_c = \frac{1}{\eta_c}$ as follows:

$$P_{source} = VI = C_c P_{elec} + P_{stdby} \tag{2}$$

in which P_{stdby} is the controller electronics losses. Equation (2) applies when electronic circuitry is preventing the controller from sending current into the battery (Verstraten et al. 2016).

4.2 | Motor Losses

This work represents the friction torque with a classical friction model which consists of coulomb friction and viscous friction. The voltage drop in the motor winding resistance is directly proportional to the current I, resulting in a power loss given by $P_{Joule} = RI^2$, where $R = R_{ref}[1 + \alpha(T - T_{ref})]$ is the total winding resistance. Here, α depicts the change in resistance with the per degree variation of temperature T (Ali, Hanif, and Ahmed 2016). Additionally, due to the proportional relation of motor current and its torque, it can be considered that the joule loss of the motor is proportional to torque squared. So, P_{Joule} becomes:

$$P_{Joule} = \alpha^T_{jl_i} \tau_i^2 \tag{3}$$

where $\alpha^T_{jl_i}$ is the joule loss coefficient of the ith motor at temperature T.

Motor friction power losses can be considered to be proportional to motor speed $\dot{\theta}_{mi}$ (Coulomb friction) and, to some extent, to $\dot{\theta}^2_{mi}$ (viscous friction). Moreover, windage losses are typically considered to be proportional to $\dot{\theta}^3_{mi}$.

Furthermore, there are losses due to the rotating magnet. They can be subdivided into two main contributions: Hysteresis losses and Eddy current losses (Hou et al. 2021). Hysteresis losses are proportional to speed $\dot{\theta}_{mi}$, similar to Coulomb friction. On the other hand, eddy current losses are proportional to $\dot{\theta}^2_{mi}$ and can be mathematically included in the viscous friction losses (Verstraten 2018).

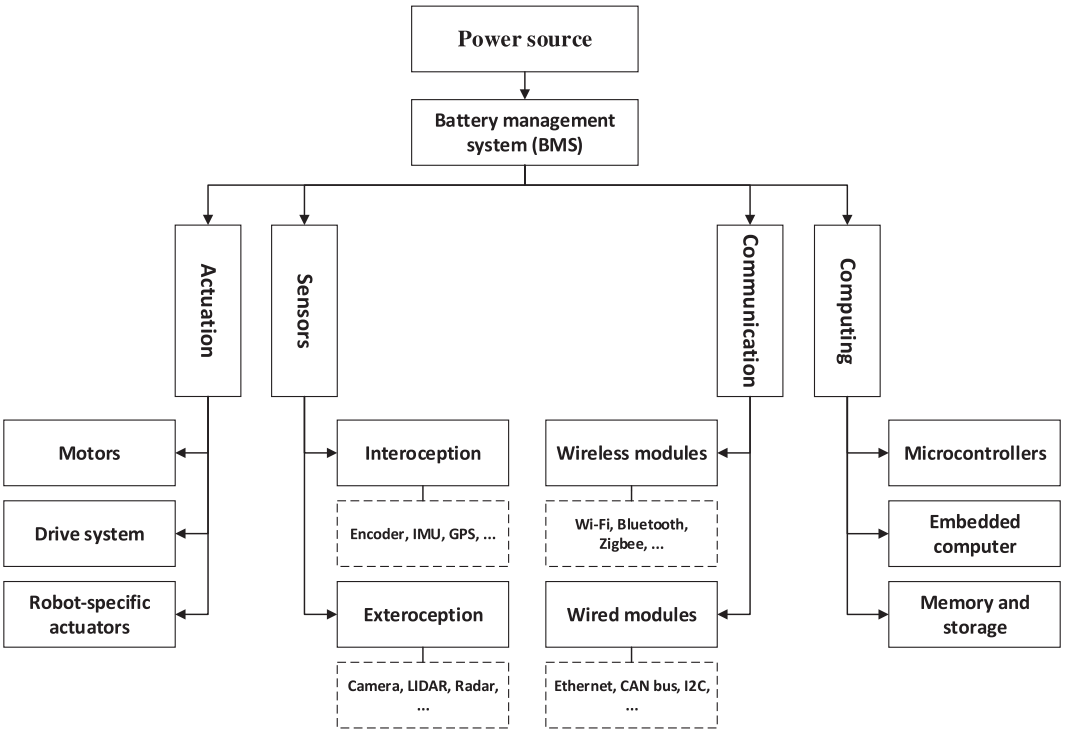

FIGURE 1 | Subsystems in power consumption breakdown of a mobile robot for energy modeling purposes.

4.3 | Gear Losses

Gearbox losses significantly impact the efficiency of a mechanical system. Moreover, constant ratio mechanical transmissions are the most commonly used gearboxes in robotic systems. Due to power losses in these gears, larger transmission ratios are required to achieve a defined torque amplification (García et al. 2020). This highlights the importance of using more efficient gears such as Garcia et al. (2022) in robotic systems and considering gear losses in energy consumption modeling of GMRs.

In this work, we assume that gearbox losses correlate directly with the input mechanical power.

$$P_{loss\,gear} = \alpha_{gl_i} \tau_{mi} \dot{\theta}_{w_i} \tag{4}$$

where α_{gl_i} is the gear loss coefficient and τ_{mi} is the mechanical torque applied on the gear.

4.4 | Robot Friction Losses and Kinetic Energy

It is well known that friction is a major source of disturbances affecting motion quality (Ferretti et al. 2003). Therefore, it must be included as an additional component in robot modeling. For wheeled mobile robots undergoing pure rolling without slipping, the rolling friction force can be expressed as

$$F_{ci} = \beta_{rf_i} \mathrm{sgn}(\dot{\theta}_{w_i}) = \frac{\mu_r M_c g}{N} \mathrm{sgn}(\dot{\theta}_{w_i}) \tag{5}$$

where μ_r is the rolling friction coefficient, dependent on the type of surface, materials, and the radius of the wheel (Wahab, Rios-Gutierrez, and El Shahat 2015). Moreover, M_c is the robot mass and N is the number of active wheels, so $\frac{M_c}{N} g$ represents the normal force on each active wheel.

Furthermore, viscous friction has a linear relation with velocity:

$$F_{vi} = \beta_{vf_i} \dot{\theta}_{w_i} \tag{6}$$

where β_{vf_i} is the viscous friction coefficient. So, the power losses due to robot friction can be expressed as

$$P_{robot\ friction} = \sum_{i=1}^{N} \left(\frac{\mu_r M_c g}{N} \mathrm{sgn}(\dot{\theta}_{w_i}) \dot{\theta}_{w_i} + \beta_{vf_i} \dot{\theta}_{w_i}^2 \right) \tag{7}$$

After deducting the losses, the remaining power available for increasing the kinetic energy and accelerating the robot is as follows:

$$\begin{aligned} P_{kinetic} = \sum_{i=1}^{N} (\max(0, I_{rroti} \ddot{\theta}_{w_i} \dot{\theta}_{w_i})) \\ + \max(0, M_c \dot{v}\, v) + \max(0, I_c \dot{\omega}\, \omega) \end{aligned} \tag{8}$$

where I_{rroti} is the rotor reflected inertia, M_c and I_c are robot mass and inertia, and v and ω represent the robot linear and angular speed, respectively.

This approach is most suitable when the controller does not facilitate power regeneration but allows braking using braking resistors. It may also be applicable when electronic circuitry prevents the controller from sending current into the battery. Such protective circuits are commonly used with batteries, which can be damaged or even explode if overcharged (Verstraten 2018).

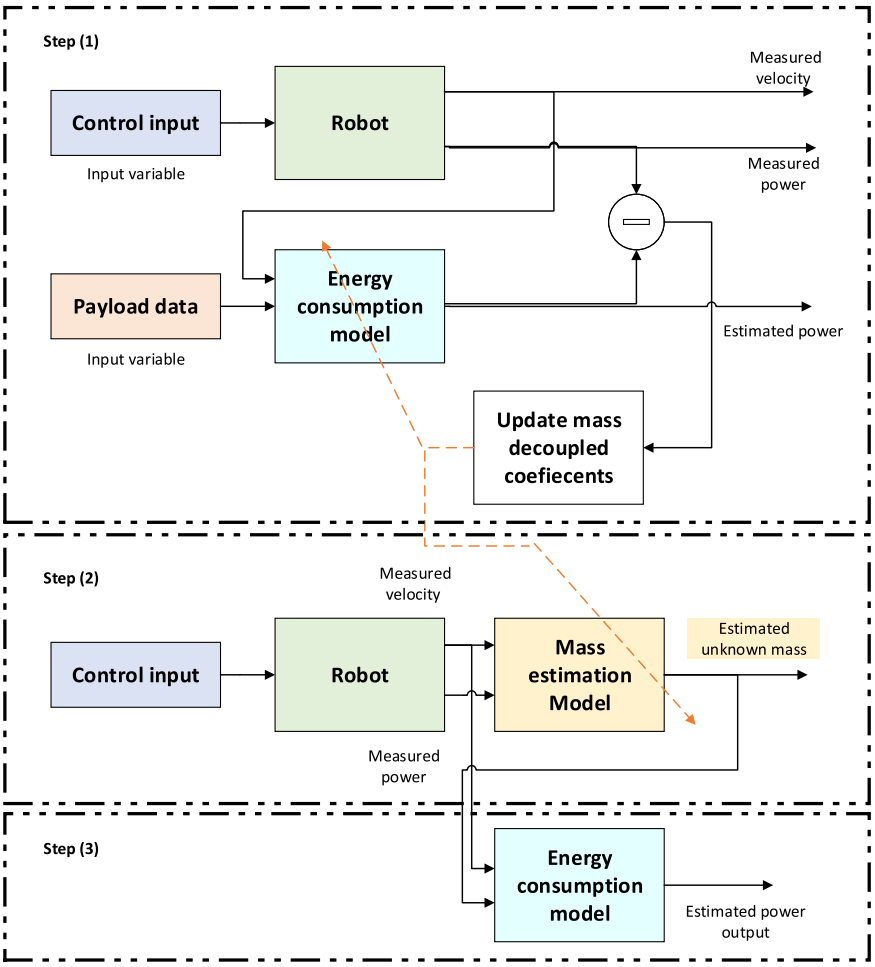

FIGURE 2 | The proposed hybrid approach for modeling actuation energy consumption in GMRs with unknown mass. Step 1: Offline estimation of mass-decoupled coefficients in actuation power model. In this step payload is a known input variable and the orange line indicates updating mass-decoupled coefficients in the energy consumption model and mass estimation model. Step 2: Online estimation of the robot's unknown payload. Step 3: Online energy consumption calculation using the parameters estimated in steps 1 and 2.

4.5 | Energy Consumption

Following the basic relationship between power and energy, we can calculate the electrical energy consumption E_{elec} from the source power P_{source}. The approach employed in this work involves the integration of positive power:

$$E_{elec} = \int \max(0, P_{source})dt = \frac{1}{2}\int (P_{source} + |P_{source}|)dt \quad (9)$$

Considering Figure 3, and Equations (3) to (8), it can be written:

$$\begin{aligned} P_{elec} &= P_{losses} + P_{kinetic} \\ &= \sum_{i=1}^{N} \Big(\alpha_{jl_i}^T \tau_i^2 + \alpha_{cf_i} \mathrm{sgn}(\dot{\theta}_{m_i}) \dot{\theta}_{m_i} + \alpha_{vf_i} \dot{\theta}_{m_i}^2 \\ &\quad + \alpha_{wl_i} \mathrm{sgn}\left(\dot{\theta}_{m_i}^3\right) \dot{\theta}_{m_i}^3 + \alpha_{hl_i} \mathrm{sgn}(\dot{\theta}_{m_i}) \dot{\theta}_{m_i} \\ &\quad + \alpha_{el_i} \dot{\theta}_{m_i}^2 + \alpha_{gl_i} \tau_{m_i} \dot{\theta}_{w_i} \Big) \\ &\quad + \sum_{i=1}^{N} \left(\frac{\mu_r M_c g}{N} \mathrm{sgn}(\dot{\theta}_{w_i}) \dot{\theta}_{w_i} + \beta_{vf} \dot{\theta}_{w_i}^2 + \max(0, I_{rrot_i} \ddot{\theta}_{w_i} \dot{\theta}_{w_i}) \right) \\ &\quad + \max(0, M_c \dot{v}\, v) + \max(0, I_c \dot{\omega}\, \omega) \end{aligned} \quad (10)$$

By defining the robot's velocity vector as $\dot{\boldsymbol{\zeta}} = [v, \omega]^T = \boldsymbol{R}\dot{\boldsymbol{\theta}}_{\boldsymbol{w}}$ where $\dot{\boldsymbol{\zeta}}$ is a function of the wheel speeds $\dot{\theta}_w = [\theta_{w1}, ..., \theta_{wN}]^T$ and given that $\dot{\theta}_{m_i} = n\dot{\theta}_{w_i}$ where n is the gear ratio, for identical motors used in a robot, we can rewrite Equation (10) as follows:

$$\begin{aligned} P_{elec} &= \sum_{i=1}^{N} \Big(\alpha_{jl}^T \tau_i^2 + \alpha_1 \mathrm{sgn}(\dot{\theta}_{w_i}) \dot{\theta}_w + \alpha_2 \dot{\theta}_{w_i}^2 \\ &\quad + \alpha_3 \mathrm{sgn}\left(\dot{\theta}_{w_i}^3\right) \dot{\theta}_{m_i}^3 + \alpha_{gl} \tau_{m_i} \dot{\theta}_{w_i} \Big) \\ &\quad + \sum_{i=1}^{N} \left(\beta_{rf} \mathrm{sgn}(\dot{\theta}_{w_i}) \dot{\theta}_{w_i} + \beta_{vf} \dot{\theta}_{w_i}^2 + \max(0, I_{rrot} \ddot{\theta}_{w_i} \dot{\theta}_{w_i}) \right) \\ &\quad + \max\left(0, \ddot{\theta}_w^T \boldsymbol{R}^T \boldsymbol{M} \boldsymbol{R} \dot{\theta}_w\right) \end{aligned} \quad (11)$$

where

$$\begin{aligned} n\left(\alpha_{cf_i} + \alpha_{hl_i}\right) &= \alpha_1 \\ n^2\left(\alpha_{vf_i} + \alpha_{el_i}\right) &= \alpha_2 \\ n^3 \alpha'_{wl_i} &= \alpha_3 \\ \begin{bmatrix} M_c & 0 \\ 0 & I_c \end{bmatrix} &= \boldsymbol{M} \end{aligned}$$

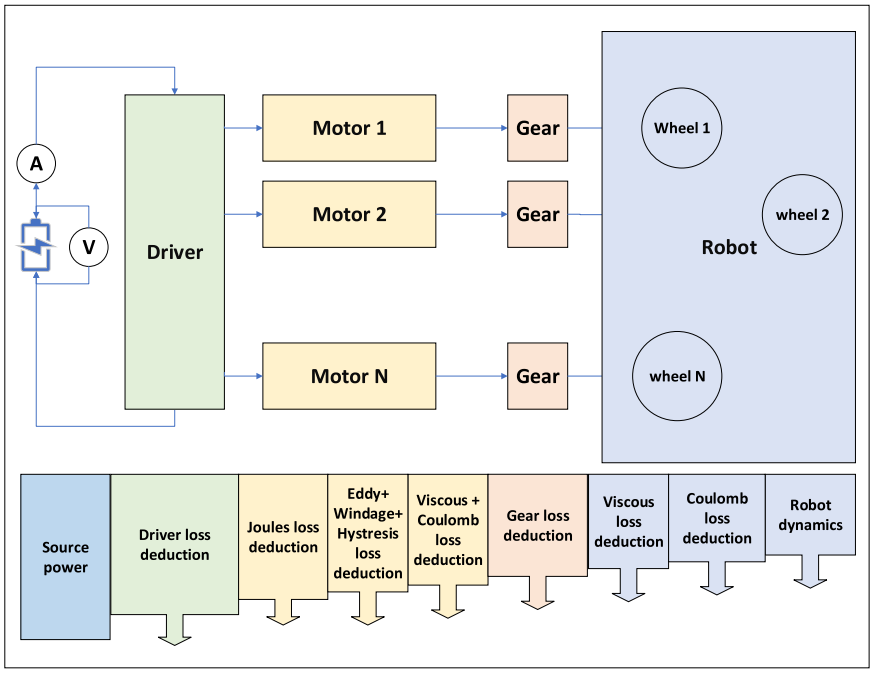

FIGURE 3 | Actuation power breakdown for mobile robots equipped with DC motors in their moving mechanisms. This breakdown allows the deduction of power losses from the power source and the evaluation of energy consumption across different parts.

By neglecting windage loss in Equation (11), P_{elec} can be expressed as:

$$\begin{aligned} P_{elec} = & \sum_{i=1}^{N} \left(\alpha_{jl}^T \tau_i^2 + \alpha_1 \text{sgn}(\dot{\theta}_{w_i}) \dot{\theta}_{w_i} + \alpha_2 \dot{\theta}_{w_i}^2 + \alpha_{gl} \tau_{m_i} \dot{\theta}_{w_i} \right) \\ & + \sum_{i=1}^{N} \Big(\beta_{rf} \text{sgn}(\dot{\theta}_{w_i}) \dot{\theta}_{w_i} + \beta_{vf} \dot{\theta}_{w_i}^2 \\ & + \frac{1}{2} I_{rrot} (\ddot{\theta}_{w_i} \dot{\theta}_{w_i} + \text{sgn}(\ddot{\theta}_{w_i} \dot{\theta}_{w_i})(\ddot{\theta}_{w_i} \dot{\theta}_{w_i})) \\ & + \frac{1}{2} \Big(\ddot{\theta}_w^T \boldsymbol{M}' \boldsymbol{\delta}^i \dot{\theta}_w + \text{sgn}\Big(\ddot{\theta}_w^T \boldsymbol{M}' \theta_w \Big) \ddot{\theta}_w^T \boldsymbol{M}' \boldsymbol{\delta}^i \dot{\theta}_w \Big) \Big) \end{aligned} \tag{12}$$

where $\boldsymbol{\delta}^i = (\delta_{jk})$ is a matrix of size N and is defined as:

$$\delta_{jk} = \begin{cases} 1 & \text{if } j = k = i \\ 0 & \text{otherwise} \end{cases} \tag{13}$$

And $\boldsymbol{M}' = \boldsymbol{R}^T \boldsymbol{M} \boldsymbol{R}$. We can obtain mechanical power p_{mi} for calculating the gear losses of each motor by the following equation:

$$\begin{aligned} p_{mi} = \tau_{mi} \dot{\theta}_{w_i} = & \beta_{rf} \text{sgn}(\dot{\theta}_{w_i}) \dot{\theta}_{w_i} + \beta_{vf} \dot{\theta}_{w_i}^2 \\ & + \frac{1}{2} I_{\text{rrot}} (\ddot{\theta}_{w_i} \dot{\theta}_{w_i} + \text{sgn}(\ddot{\theta}_{w_i} \dot{\theta}_{w_i})(\ddot{\theta}_{w_i} \dot{\theta}_{w_i})) \\ & + \frac{1}{2} \Big(\ddot{\theta}_w^T \boldsymbol{M}' \boldsymbol{\delta}^i \dot{\theta}_w + \text{sgn}\Big(\ddot{\theta}_w^T \boldsymbol{M}' \boldsymbol{\delta}^i \dot{\theta}_w \Big) \ddot{\theta}_w^T \boldsymbol{M}' \boldsymbol{\delta}^i \dot{\theta}_w \Big) \end{aligned} \tag{14}$$

so Equation (12) can be represented as follows:

$$\begin{aligned} P_{\text{elec}} = & \sum_{i=1}^{N} \left(\alpha_{jl}^T \tau_i^2 + \gamma_1 \text{sgn}(\dot{\theta}_{w_i}) \dot{\theta}_{w_i} + \gamma_2 \dot{\theta}_{w_i}^2 \right) \\ & + \gamma_3 (\ddot{\theta}_{w_i} \dot{\theta}_{w_i} + \text{sgn}(\ddot{\theta}_{w_i} \dot{\theta}_{w_i})(\ddot{\theta}_{w_i} \dot{\theta}_{w_i})) \\ & + \gamma_4 \Big(\ddot{\theta}_w^T \boldsymbol{M}' \boldsymbol{\delta}^i \dot{\theta}_w + \text{sgn}\Big(\ddot{\theta}_w^T \boldsymbol{M}' \boldsymbol{\delta}^i \dot{\theta}_w \Big) \ddot{\theta}_w^T \boldsymbol{M}' \boldsymbol{\delta}^i \dot{\theta}_w \Big) \end{aligned} \tag{15}$$

where

$$\begin{aligned} \alpha_1 + (\alpha_{gl} + 1)\beta_{rf} &= \gamma_1 \\ \alpha_2 + (\alpha_{gl} + 1)\beta_{vf} &= \gamma_2 \\ (\alpha_{gl} + 1)\frac{1}{2} I_{\text{rrot}} &= \gamma_3 \\ (\alpha_{gl} + 1)\frac{1}{2} &= \gamma_4 \end{aligned}$$

To estimate the joule losses based on Equation (3), motor torque τ_i needs to be calculated. It can be shown that $\ddot{\theta}_w^T \boldsymbol{M}' \boldsymbol{\delta}^i \dot{\theta}_w = \ddot{\theta}_w^T \boldsymbol{M}' \boldsymbol{\Psi}^i \dot{\theta}_{w_i}$ where $\boldsymbol{\Psi}^i = \frac{\boldsymbol{\delta}^i \dot{\theta}_w}{\dot{\theta}_{w_i}}$. Considering the basic relation between torque and power $\tau = \frac{P}{\dot{\theta}}$ and Equation (15), we have

$$\begin{aligned} \tau_i = & \gamma_1 \text{sgn}(\dot{\theta}_{w_i}) + \gamma_2 \dot{\theta}_{w_i} + \gamma_3 \Big(1 + \text{sgn}(\ddot{\theta}_{w_i} \dot{\theta}_{w_i}) \Big) \ddot{\theta}_{w_i} \\ & + \gamma_4 \Big(1 + \text{sgn}\Big(\ddot{\theta}_{w_i}^T \boldsymbol{M}' \boldsymbol{\delta}^i \dot{\theta}_w \Big) \Big) \ddot{\theta}_w^T \boldsymbol{M}' \boldsymbol{\Psi}^i \end{aligned} \tag{16}$$

Now by replacing $\alpha_{jl}^T \tau_i^2$ using Equation (16) and considering Equation (2), after simplifying, we obtain

$$\begin{aligned} P_{\text{source}} = & P_{\text{stdby}} + \sum_{i=1}^{N} \Big(\sigma_0 + \sigma_1 \dot{\theta}_{w_i}^2 \\ & + \sigma_2 \Big(2 + \text{sgn}(\ddot{\theta}_{w_i} \dot{\theta}_{w_i}) \Big) \ddot{\theta}_{w_i}^2 \\ & + \sigma_3 \Big(2 + \text{sgn}\Big(\ddot{\theta}_w^T \boldsymbol{M}' \boldsymbol{\delta}^i \dot{\theta}_w \Big) \Big) \Big(\ddot{\theta}_w^T \boldsymbol{M}' \boldsymbol{\Psi}^i \Big)^2 \\ & + \sigma_4 \text{sgn}(\dot{\theta}_{w_i}) \dot{\theta}_{w_i} \\ & + \sigma_5 \Big(1 + \text{sgn}(\ddot{\theta}_{w_i} \dot{\theta}_{w_i}) \Big) \text{sgn}(\dot{\theta}_{w_i}) \ddot{\theta}_{w_i} \\ & + \sigma_6 \Big(1 + \text{sgn}\Big(\ddot{\theta}_w^T \boldsymbol{M}' \boldsymbol{\delta}^i \dot{\theta}_w \Big) \Big) \text{sgn}(\dot{\theta}_{w_i}) \ddot{\theta}_w^T \boldsymbol{M}' \boldsymbol{\Psi}^i \\ & + \sigma_7 \Big(1 + \text{sgn}(\ddot{\theta}_{w_i} \dot{\theta}_{w_i}) \Big) \ddot{\theta}_{w_i} \dot{\theta}_{w_i} \\ & + \sigma_8 \Big(1 + \text{sgn}\Big(\ddot{\theta}_w^T \boldsymbol{M}' \boldsymbol{\delta}^i \dot{\theta}_w \Big) \Big) \ddot{\theta}_w^T \boldsymbol{M}' \boldsymbol{\delta}^i \dot{\theta}_w \\ & + \sigma_9 \Big(1 + \text{sgn}(\ddot{\theta}_{w_i} \dot{\theta}_{w_i}) \Big) \Big(1 + \text{sgn}\Big(\ddot{\theta}_w^T \boldsymbol{M}' \boldsymbol{\delta}^i \dot{\theta}_w \Big) \Big) \Big(\ddot{\theta}_w^T \boldsymbol{M}' \boldsymbol{\Psi}^i \Big) \ddot{\theta}_{w_i} \Big) \end{aligned} \tag{17}$$

where

$$\begin{aligned}
\alpha_{jl}^T\gamma_1^2 C_c &= \sigma_0\\
\left(\gamma_2 + \alpha_{jl}^T\gamma_2^2\right)C_c &= \sigma_1\\
2\alpha_{jl}^T\gamma_3^2 C_c &= \sigma_2\\
2\alpha_{jl}^T\gamma_4^2 C_c &= \sigma_3\\
\left(\gamma_1 + 2\alpha_{jl}^T\gamma_1\gamma_2\right)C_c &= \sigma_4\\
2\alpha_{jl}^T\gamma_1\gamma_3 C_c &= \sigma_5\\
2\gamma_1\gamma_4 C_c &= \sigma_6\\
\left(2\alpha_{jl}^T\gamma_2\gamma_3 + \gamma_3\right)C_c &= \sigma_7\\
\left(2\alpha_{jl}^T\gamma_2\gamma_4 + \gamma_4\right)C_c &= \sigma_8\\
2\alpha_{jl}^T\gamma_3\gamma_4 C_c &= \sigma_9
\end{aligned}$$

To derive mass-decoupled parameters in Equation (17), as $\gamma_1 = (\alpha_{cf_i} + \alpha_{hl_i}) + (\alpha_{gl} + 1)\beta_{rf}$, we substitute it with a linear equation $\gamma_1 = \alpha_0 + \alpha_1 m$. Factoring the mass parameter, Equation (17) can be rewritten:

$$\begin{aligned}
P_{source} = P_{stdby} + \sum_{i=1}^{N}&(\beta_0 + \beta_1 m + \beta_2 m^2\\
&+ \beta_3\dot{\theta}_{w_i}^2 + \beta_4\left(2 + \mathrm{sgn}(\ddot{\theta}_{w_i}\dot{\theta}_{w_i})\right)\ddot{\theta}_{w_i}^2\\
&+ \beta_5 m\left(2 + \mathrm{sgn}\left(\ddot{\theta}_w^T\boldsymbol{M}''\boldsymbol{\delta}^i\dot{\boldsymbol{\theta}}_w\right)\right)\left(\ddot{\theta}_w^T\boldsymbol{M}''\boldsymbol{\Psi}^i\right)^2\\
&+ \beta_6\mathrm{sgn}(\dot{\theta}_{w_i})\dot{\theta}_{w_i} + \beta_7 m\mathrm{sgn}(\dot{\theta}_{w_i})\dot{\theta}_{w_i}\\
&+ \beta_8\left(1 + \mathrm{sgn}(\ddot{\theta}_{w_i}\dot{\theta}_{w_i})\right)\mathrm{sgn}(\dot{\theta}_{w_i})\ddot{\theta}_{w_i}\\
&+ \beta_9 m\left(1 + \mathrm{sgn}(\ddot{\theta}_{w_i}\dot{\theta}_{w_i})\right)\mathrm{sgn}(\dot{\theta}_{w_i})\ddot{\theta}_{w_i}\\
&+ \beta_{10} m\left(1 + \mathrm{sgn}\left(\ddot{\theta}_w^T\boldsymbol{M}''\boldsymbol{\delta}^i\dot{\boldsymbol{\theta}}_w\right)\right)\mathrm{sgn}(\dot{\theta}_{w_i})\ddot{\theta}_w^T\boldsymbol{M}''\boldsymbol{\Psi}^i\\
&+ \beta_{11} m^2\left(1 + \mathrm{sgn}\left(\ddot{\theta}_w^T\boldsymbol{M}''\boldsymbol{\delta}^i\dot{\boldsymbol{\theta}}_w\right)\right)\mathrm{sgn}(\dot{\theta}_{w_i})\ddot{\theta}_w^T\boldsymbol{M}''\boldsymbol{\Psi}^i\\
&+ \beta_{12}\left(1 + \mathrm{sgn}(\ddot{\theta}_{w_i}\dot{\theta}_{w_i})\right)\ddot{\theta}_{w_i}\dot{\theta}_{w_i}\\
&+ \beta_{13} m\left(1 + \mathrm{sgn}\left(\ddot{\theta}_w^T\boldsymbol{M}''\boldsymbol{\delta}^i\dot{\boldsymbol{\theta}}_w\right)\right)\ddot{\theta}_w^T\boldsymbol{M}''\boldsymbol{\delta}^i\dot{\boldsymbol{\theta}}_w\\
&+ \beta_{14} m\left(1 + \mathrm{sgn}(\ddot{\theta}_{w_i}\dot{\theta}_{w_i})\right)\\
&\left(1 + \mathrm{sgn}\left(\ddot{\theta}_w^T\boldsymbol{M}''\boldsymbol{\delta}^i\dot{\boldsymbol{\theta}}_w\right)\right)\left(\ddot{\theta}_w^T\boldsymbol{M}''\boldsymbol{\Psi}^i\right)\ddot{\theta}_{w_i}\Big)
\end{aligned} \tag{18}$$

where $m\boldsymbol{M}'' = \boldsymbol{M}'$ and β_0 to β_{14} are positive coefficients that can be computed from Equation (17) by following the basic mathematics calculations. in this work, we refer β_0 to β_{14} as mass-decoupled coefficients.

5 | Hybrid Parameters Estimation Approach

As described in Section 3 and shown in Figure 2, the methodology of the presented work contains three main steps. The following subsections provide a detailed discussion of each step.

5.1 | Offline Mass-Decoupled Coefficients Estimation

In the first step, the mass-decoupled coefficients $\beta_0, ..., \beta_{14}$ in Equation (18) are estimated using an off-line approach. For this purpose, the multiple linear regression model of Equation (18) is constructed as follows:

$$\overbrace{\begin{bmatrix} p_1\\ p_2\\ \vdots\\ p_k\end{bmatrix}}^{\boldsymbol{P}} = \overbrace{\begin{bmatrix} X_1^0 & X_1^1 & \dots & X_1^{14}\\ X_2^0 & X_2^1 & \dots & X_2^{14}\\ \vdots & \vdots & \ddots & \vdots\\ X_k^0 & X_k^1 & \dots & X_k^{14}\end{bmatrix}}^{\boldsymbol{X}}\overbrace{\begin{bmatrix}\beta_0\\ \beta_1\\ \vdots\\ \beta_{14}\end{bmatrix}}^{\boldsymbol{\beta}} \tag{19}$$

In this regression model, k is the number of the measurements. Considering Equation (18) and neglecting changes in temperature of motor windings, the first regressor is $X^0 1$, $\{X^1, X^2\} = f(m, m^2)$ are functions of robot mass, $\{X^3, X^4, X^6, X^8, X^{12}\} = f(\dot{\theta}, \ddot{\theta})$ are functions of the measured wheels' speed (and acceleration). The rest of the regressors are functions of both mass and wheels' speed. Moreover, $p_k = p_{k_{source}} - p_{k_{stdby}}$ where $p_{k_{source}}$ is source power measuring and $p_{k_{stdby}}$ is the controller electronics losses as described in Section 4.

To ensure a rich data set for the estimation of the model parameters, it is necessary to drive the GMR under various payload conditions. The selection of the robot's payload for this step typically relies on the specific operating conditions and mission requirements of the GMR. It is recommended to obtain measured data in two conditions: no-load and full-load. Furthermore, the robot should be driven with different speeds and acceleration profiles.

The step of finding the best estimation of mass-decoupled coefficients $\hat{\boldsymbol{\beta}}$ can be formulated as an optimization problem, where the optimization cost function is

$$\min\left\{\frac{1}{k}(\boldsymbol{P} - \boldsymbol{X}\hat{\boldsymbol{\beta}})^T(\boldsymbol{P} - \boldsymbol{X}\hat{\boldsymbol{\beta}}) : \hat{\beta}_i > 0\right\} \tag{20}$$

In this work, the projected gradient descent algorithm is employed to solve the optimization problem in Equation (20) (Goldstein 1964; Calamai and Moré 1987). A brief description of this algorithm is provided in Section 5.1.1.

5.1.1 | Projected Gradient Descent Algorithm

The projected gradient descent method (PGD), introduced in (Goldstein 1964) to solve the general problem of minimizing a continuously differentiable mapping $f: \boldsymbol{R^N} \to \boldsymbol{R}$ on a nonempty closed convex set $\Omega \subset \boldsymbol{R^N}$:

$$\min\{f(\beta) : \beta \subset \Omega\} \tag{21}$$

In our estimation problem, projected gradient descent is concerned with the case where Ω is defined by bounded constraints.

$$\Omega = \{\beta \in \boldsymbol{R^N} : l_i \le \beta_i \le u_i\} \tag{22}$$

Where l_i and u_i are constraints on the mass decoupled coefficients in Equation (19).

Given an inner product norm $\|.\|$ and a nonempty closed convex set Ω, the projection into Ω is the mapping $\boldsymbol{P}: \boldsymbol{R^N} \to \Omega$ which

is a projection operator, and itself is also an optimization problem (Calamai and Moré 1987), defined by

$$P_\Omega(\beta) = \arg\min\{\|z - \beta\| : z \in \Omega\} \tag{23}$$

The general framework for projected gradient descent proposed by Reddi, Kale, and Kumar (2019) is shown in Algorithm 1. In our work, the adaptive method of root mean square propagation (RMSProp) is used to enhance convergence speed by maintaining an exponentially weighted average of the squares of past gradients (Liang, Ma, and Li 2020). RMSProp then divides the learning rate by this average to speed up convergence. In this method, ϕ_k in Algorithm 1 is gradient of cost function $\phi_k = g_k$ and $\psi_k = (1-c)\text{diag}(\sum_{i=1}^{k} c^{k-i} g_i^2)$, where momentum coefficient c can be chosen between [0.9, 0.99].

Algorithm 1 Generic Framework of PGD

Choosing an initial guess: β_0 in Ω and Learning rate: α

$k, k+1 \in \mathbb{N}$: current and next iteration counter

β_k, β_{k+1}: current and next variable

1: **while** stopping criterion not met **do**

2: $g_k = \nabla f(\beta_k)$

3: $m_k = \phi_k(g_1, ..., g_k)$

4: $V_k = \psi_k(g_1, ..., g_k)$

5: $\alpha_k = \alpha/\sqrt{k}$

6: $\beta_{k+\frac{1}{2}} = \beta_k - \alpha_k m_k/\sqrt{V_k}$

7: $\beta_{k+1} = P_\Omega(\beta_{k+\frac{1}{2}})$

8: **end while**

5.2 | Online Unknown Payload Estimation

For the second step of the proposed approach, it is needed to reformulate Equation (18) as a quadratic equation with respect to mass parameter m. Therefore, considering that the mass-decoupled coefficients have been estimated in the first step, we have

$$\begin{aligned}
&\sum_{i=1}^{N}\left(\beta_2 + \beta_{11}\left(1+\text{sgn}\left(\ddot{\theta}_w^T \boldsymbol{M}''\boldsymbol{\delta}^i\dot{\theta}_w\right)\right)\text{sgn}(\dot{\theta}_{w_i})\ddot{\theta}_w^T\boldsymbol{M}''\boldsymbol{\Psi}^i\right)m^2\\
&+\sum_{i=1}^{N}\left(\beta_1+\beta_5\left(2+\text{sgn}\left(\ddot{\theta}_w^T\boldsymbol{M}''\boldsymbol{\delta}^i\dot{\theta}_w\right)\right)\left(\ddot{\theta}_w^T\boldsymbol{M}''\boldsymbol{\Psi}^i\right)^2\right.\\
&+\beta_7\text{sgn}(\dot{\theta}_{w_i})\dot{\theta}_{w_i}\\
&+\beta_9\left(1+\text{sgn}(\ddot{\theta}_{w_i}\dot{\theta}_{w_i})\right)\text{sgn}(\dot{\theta}_{w_i})\ddot{\theta}_{w_i}\\
&+\beta_{10}\left(1+\text{sgn}\left(\ddot{\theta}_w^T\boldsymbol{M}''\boldsymbol{\delta}^i\dot{\theta}_w\right)\right)\text{sgn}(\dot{\theta}_{w_i})\ddot{\theta}_w^T\boldsymbol{M}''\boldsymbol{\Psi}^i\\
&+\beta_{13}\left(1+\text{sgn}\left(\ddot{\theta}_w^T\boldsymbol{M}''\boldsymbol{\delta}^i\dot{\theta}_w\right)\right)\ddot{\theta}_w^T\boldsymbol{M}''\boldsymbol{\delta}^i\dot{\theta}_w\\
&+\beta_{14}\left(1+\text{sgn}(\ddot{\theta}_{w_i}\dot{\theta}_{w_i})\right)\\
&\quad\left.\left(1+\text{sgn}\left(\ddot{\theta}_w^T\boldsymbol{M}''\boldsymbol{\delta}^i\dot{\theta}_w\right)\right)\left(\ddot{\theta}_w^T\boldsymbol{M}''\boldsymbol{\Psi}^i\right)\ddot{\theta}_{w_i}\right)m\\
&+\sum_{i=1}^{N}\left(\beta_0+\beta_3\dot{\theta}_{w_i}^2+\beta_4\left(2+\text{sgn}(\ddot{\theta}_{w_i}\dot{\theta}_{w_i})\right)\ddot{\theta}_{w_i}^2+\beta_6\text{sgn}(\dot{\theta}_{w_i})\dot{\theta}_{w_i}\right.\\
&+\beta_8\left(1+\text{sgn}(\ddot{\theta}_{w_i}\dot{\theta}_{w_i})\right)\text{sgn}(\dot{\theta}_{w_i})\ddot{\theta}_{w_i}\\
&\left.+\beta_{12}\left(1+\text{sgn}(\ddot{\theta}_{w_i}\dot{\theta}_{w_i})\right)\ddot{\theta}_{w_i}\dot{\theta}_{w_i}\right)\\
&+P_{\text{stdby}}-P_{\text{source}}=0
\end{aligned} \tag{24}$$

Equation (24) is in the standard form of quadratic equations $am^2 + bm + c = 0$. The acceptable solution for the Equation (24) must be a real positive value within the range of the no-load and full-load robot mass. Therefore, the estimated mass $\hat{m} \in S$ is as follows:

$$S = \{\hat{m} | m_{no\text{-}load} \le \hat{m} \le m_{full\text{-}load}, \hat{m} > 0\} \tag{25}$$

Due to the presence of noise in the system and measurements, it is recommended to find the roots of Equation (24) multiple times over a timeframe with sufficient measured data to enhance the accuracy of parameter estimation $\hat{m}$. Moreover, Equation (24) is valid for mass estimation when the robot moves. So

$$\hat{m} = \frac{\sum_{i=1}^{j} \bar{W}_i \hat{m}_i}{\sum_{i=1}^{j} \bar{W}_i} \tag{26}$$

in Equation (26), the parameter j represents the number of samples used to compute the weighted average. We proposed to use $\bar{W}_i = \frac{1}{N}\sum_{i=1}^{N}|\dot{\theta}_{w_i}|$ as the weight function, thereby the measurements in low speeds have less influence in mass estimation.

In the framework of the proposed hybrid approach for this work, the mass estimation step needs to be (re)done when the GMR payload is changed. The execution time of this step depends on the nature of the robot's operation. If there is a consistent pattern in the change of loads or the assignment of tasks, then the second step can be repeated at the start of each task. Otherwise, if there is no consistent pattern, the second step can be carried out periodically with a predefined time interval. In such cases, the power consumption estimation in step three may come with an extra error. This error represents the trade-off that should be made in the absence of precise information regarding the payload changing time. The described cases are shown in Figure 4.

It's important to note that, in addition to the mentioned power estimation error, extra energy is consumed not only for measuring the power but also for the computations involved in the data processing. Therefore, there is also another trade-off between the chosen time interval for recalibrating the mass estimation and its energy cost, which should be considered.

5.3 | Online Calculation of Actuation Power Consumption

Step three in our hybrid parameters estimation approach involves the online calculation of actuation power. In this step of the proposed power estimation method, at each sample time, the wheels' velocity is gathered either directly from the wheels or motors encoders' measurements or computationally calculated using other available sensory information, such as IMU sensors and the robot's basic structural information, including the rotation matrix $\boldsymbol{R}$. If the proposed approach is used for predicting the robot's actuation power, commanded velocities will be used. After obtaining the updated value of the estimated mass from the output of the second step in our approach, regressors $X^1, ..., X^{14}$ are calculated. Then, using the estimated

mass-decoupled coefficients $\hat{\beta}_0, ..., \hat{\beta}_{14}$ and Equations (18) or (19) the estimated actuation power is calculated.

The overall sequence of steps for the proposed hybrid parameter estimation framework is shown in Algorithm 2.

Algorithm 2 Proposed hybrid parameters estimation framework

Offline mass-decoupled coefficients estimation:

1: Measuring consumed power p_k and wheels' velocity $\dot{\theta}_i$

2: Constructing regression model from Equation (19) using measured data and initial knowledge of robot's mass matrix $\boldsymbol{M}''$ and Equation (18)

3: Estimation of mass-decoupled coefficients using the Algorithm 1

4: **Return**: mass-decoupled coefficients

Online unknown payload estimation:

5: Choose a T-second weighted average time window

6: **if** Payload change time is determined **then**

7: **for** *time* $< T$ at beginning of each task **do**

8: Form the quadratic Equations (24)

9: Calculate the weighted moving average of Equation (26) which satisfies Equation (25)

10: **end for**

11: **else**

12: Choose the periodic interval if D-second

13: **for** *time* $< T$ at beginning of each D-second interval **do**

14: Repeat steps 8 and 9

15: **end for**

16: **end if**

17: **Return**: Estimated mass

Online calculation of actuation power consumption:

18: **while** Robot mission is not finished **do**

19: Update the estimated values from steps 4 and 17

20: Estimate the actuation power consumption using Equation (18)

21: **end while**

6 | Simulation

In this section, we perform simulations to demonstrate the effectiveness of our proposed approach. The power consumption model introduced in Section 4 is applicable to GMRs without slipping in their motion. Additionally, for implementing Equation (18) primary knowledge of robot kinematics is sufficient.

For the simulation, we considered the kinematics of an indoor differential drive robot, specifically the TurtleBot3 (Burger), to establish the actuation power model. The robot is a ROS-based mobile platform designed for education, research, and prototyping, with a focus on simultaneous localization and mapping (SLAM), navigation, and manipulation capabilities (Amsters and Slaets 2020). The characteristics of the simulated robot are detailed in Table 2. To derive the actuation power, the robot's dynamics were simulated in Matlab Simulink (R2023a) with a fix-step sample time of 0.001, using the parameters in Table 3. The parameters are chosen to match the actual power output range of the robot's motors.

Furthermore, in this simulation, we set the rolling friction coefficient to $\mu_r = 0.032$, and consider a maximum payload of 5 kg. Additionally, a bounded Gaussian white noise is added to the wheels' velocity measurements in the control loop.

To generate the test and training data sets, different velocity profiles have been applied as input to each of the simulated motors. Considering the prohibition of electrical power regeneration in the motor drives, the actuation powers of the simulated motors are summed together to produce the simulated actuation power. The wheels' speed profile and simulated actuation powers are shown in Figure 5. Furthermore, during the training phase, a 5 kg payload is added at $t = 100$s, transitioning the robot state from no-load to full-load. In the test data set, the initial payload is 2 kg, and it changes to 3 kg at $t = 50$s, resulting in a total mass change from 3 to 4 kg, including the robot mass.

As discussed in Section 5, the first step of the proposed approach involves creating the regression model using the training data set, as expressed in Equation (19). Subsequently, the described PGD method outlined in Algorithm 1 is employed. Here, a similar learning rate ($\alpha = 0.001$) is applied to all the regressors, and a momentum coefficient of $c = 0.9$ is used to estimate the mass-decoupled coefficients $\beta_0, ..., \beta_{14}$ in Equation (18).

In the second step, the test data is used to estimate the robot mass by solving the quadratic equation in Equation (24) using a 10s time window at the beginning of the GMR test mission. The estimated mass $\hat{m} = 3.17$ for this time window, indicating a 5.6% error in the mass estimation (see Figure 6). Similarly, performing the mass estimation after the payload change results in $\hat{m} = 4.22$ which has a 5.5% error.

To implement the third step of our proposed approach on the test data set, we utilize Equation (18) with the mass-decoupled coefficients obtained in step one and the estimated mass from step two ($\hat{m} = 3.17, 4.22$). The estimated actuation power for test data is shown in Figure 5c, and the prediction validation is illustrated in Figure 7. These figures show that the estimation error is bounded. In our simulation mean absolute percentage error (MAPE) and R^2 score are used to evaluate the estimation accuracy, as defined in Chicco, Warrens, and Jurman (2021):

$$R^2 = 1 - \frac{\sum_{i=1}^{n}(y_i - \hat{y}_i)^2}{\sum_{i=1}^{n}(y_i - \bar{y})^2}, \qquad \text{MAPE} = \frac{1}{n}\sum_{i=1}^{n}\left|\frac{y_i - \hat{y}_i}{y_i}\right| \times 100\%. \tag{27}$$

The best possible R^2s score is 1.0 and a value of 0 means that the model predicts 0% of the relationship between the dependent and independent variables. The MAPE and R^2*score* of the estimation in the described simulation scenario are 4.3% and 0.973, respectively.

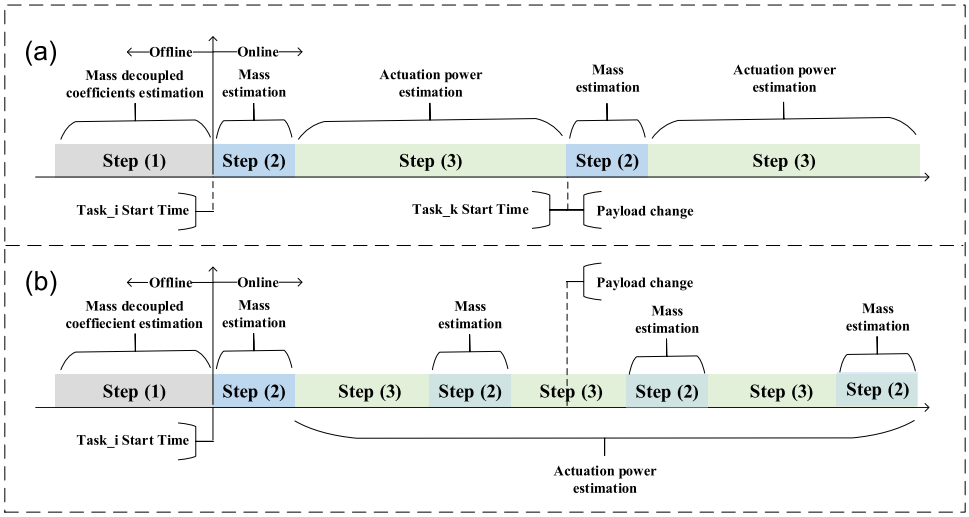

FIGURE 4 | Recalibrating mass estimation in the proposed hybrid parameters estimation approach when payload change time is determined in (a) or is undetermined in (b). When the payload change time is undetermined, mass estimation is performed periodically in predefined timeframes. This periodic recalibration may result in an additional error in power consumption due to inaccuracy in mass estimation.

TABLE 2 | Physical parameters of TurtleBot3 Burger.

Parameter	Values
Turning radius	80 mm
Wheels radius	33 mm
Maximum linear velocity	0.22 m/s
Maximum angular velocity	2.84 rad/s
Mass (no-load)	1 kg

7 | Experimental Validation

To experimentally validate the proposed power consumption method, we developed the TurtleBot's firmware to use power metering sensors. These sensors utilize the *TI INA219*, which is a zero temperature drift current/power monitoring chip (INA219 Zero Drift 2015). This module offers high resolution and accuracy, achieving a maximum relative error of $\pm 0.2\%$ after manual calibration. In our setup, the power measurement sensors are connected to the *OpenCr* control board through the I^2C interface. Instantaneous powers for components such as the battery, motors, Raspberry Pi, and lidar sensor are measured at an approximate sample rate of 20 Hz. During the implementation and development of custom messages and in selecting the data publishing frequency for additional sensors, it is necessary to consider the total and available communication bandwidth between the *OpenCr* board and the Raspberry Pi, as well as over the WiFi connection between the Raspberry Pi and the remote PC. The equipped robot's power measurements breakdown is shown in Figure 8.

7.1 | Implementation of Proposed Method

To collect the required data robot is driven with a predefined linear and angular velocity profile. This profile ensures that the robot traverses both straight and curved paths at varying speeds and for the train data set preferably covers the whole range of motors' actuation velocities. In the conducted experiments the floor surface type remained constant throughout the tests (carpet floor) and flat road grade. During the robot's movement, three different weights are placed on it as a payload to be carried. Consequently, the collected data set includes four different scenarios, no-load, 2, 3, and 5 kg payloads. In this experiment, the 5 kg payload is considered as the full-load condition.

The measured instance power of the robot during both no-load and full-load movement is shown in Figure 9a. Additionally, the total power consumption for sensing, computing, and communication, along with the power consumption for robot actuation, are illustrated in the same figure. This power consumption breakdown aligns with Equation (1) and the power measuring setup shown by the diagram in Figure 8. As mentioned in Section 3, when the robot's configuration and settings remain unchanged during a robotic mission, $P_{sen} + P_{com} + P_{comm}$ remains approximately constant for the defined mission. In such cases, Equation (1) can be expressed as

$$P = P_{static} + P_{act} \tag{28}$$

So, the problem of estimating the power consumption of our GMR can be subdivided into determining the best probabilistic estimation for P_{static} and estimating P_{act} using the proposed approach in Section 4.

To find the best probability distribution function for estimation P_{static}, its histogram data is considered. Figure 9b shows a Gaussian probability distribution with the expected value $\mu = 6.393$ and standard division $\sigma = 0.29$ can be fitted on these data. So, the estimation of static power is

$$\hat{P}_{static} = f(p|\mu, \sigma) = \frac{1}{\sigma\sqrt{2\pi}} e^{-\frac{(p-\mu)^2}{2\sigma^2}} \tag{29}$$

The steps taken to estimate the actuation power P_{act} in this section are the same as those presented in the simulation

TABLE 3 | Simulated motor parameters.

Parameter	Values	Parameter	Values
Viscous friction coefficient	2×10^{-7}Nm/(rad/s)	Resistance	0.75 Ω
Shaft inertia	1.2182×10^{-5}kgm^2	Inductance	0.00072H
Torque constant	0.037Nm/A	Electrical constant	0.0072 (rad/s)/V
Gear ratio	1:258.5	Gearbox efficiency	75%

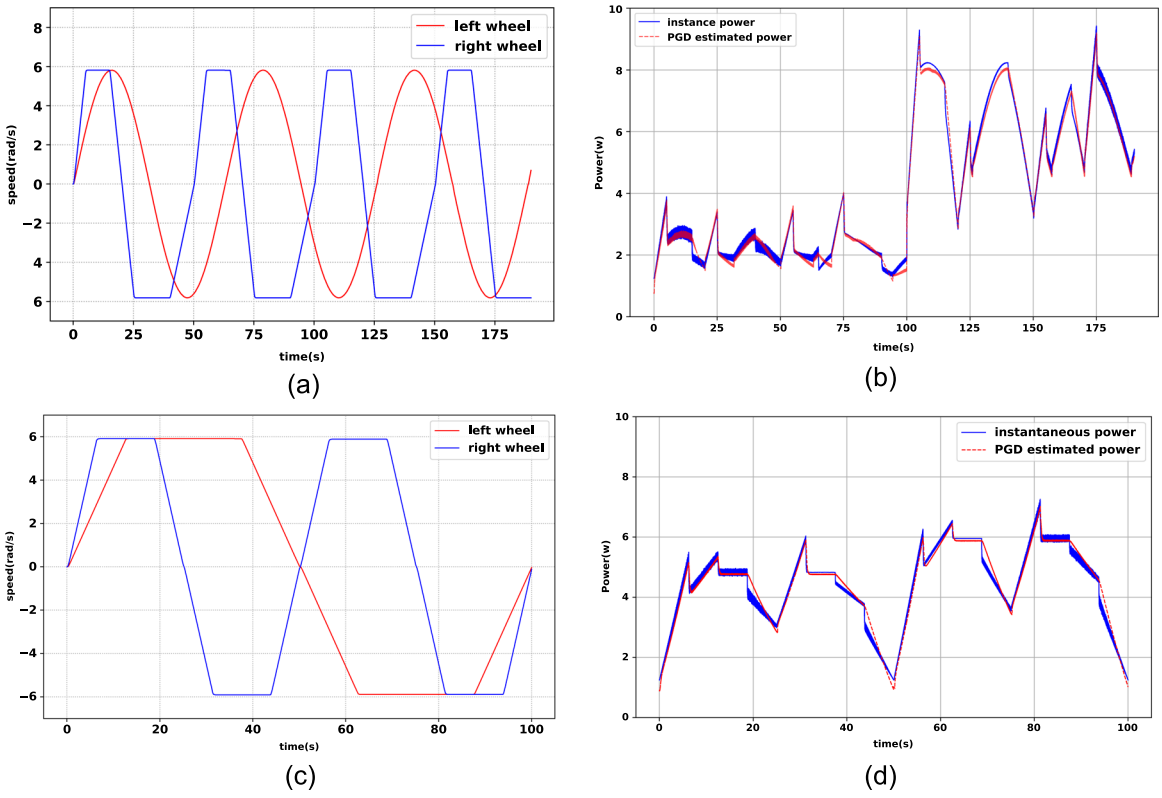

FIGURE 5 | Wheels' speed profiles for train (a) and test (c) data sets. The wheels' speed profiles are chosen to be different for test and train data sets to ensure that the model is not trained for a specific speed profile. Predicated versus simulated actuation power for the training data set (b) with a load change (no-load to full-load) at $t = 100$s and test data set with a total mass change from 3 to 4 kg at $t = 50$s (d).

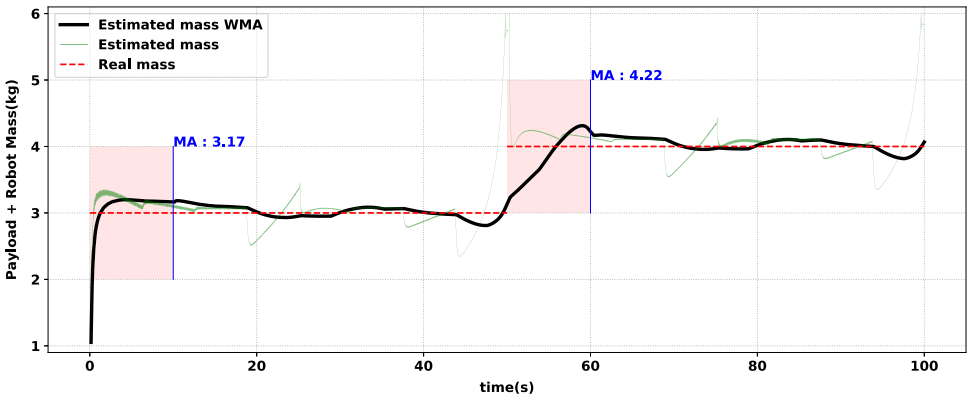

FIGURE 6 | Ground mobile robot (GMR) payload estimation for simulated test data set with a 10-s time window weighted moving average (WMA) over the estimated mass. The accuracy of mass estimation depends on selecting the time intervals to perform the mass estimation. The maximum error occurs when the wheels' speeds are significantly low.

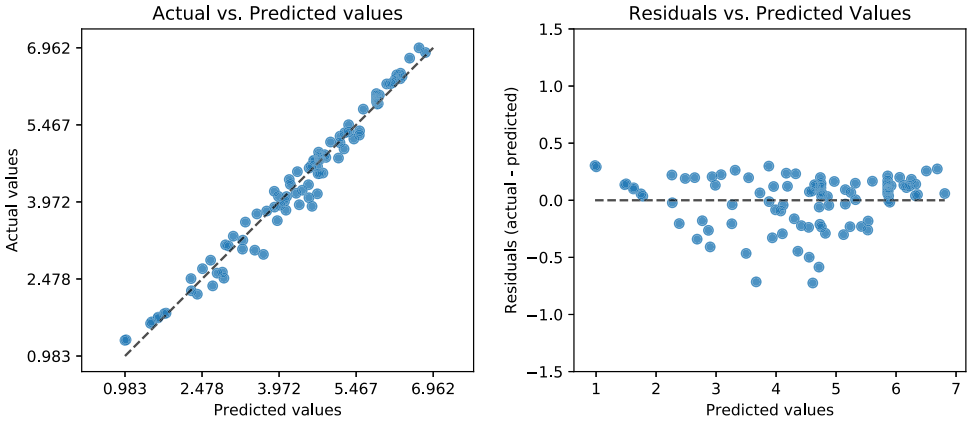

FIGURE 7 | Predictions validation of test data set in simulation. Figures show a bounded error for estimation.

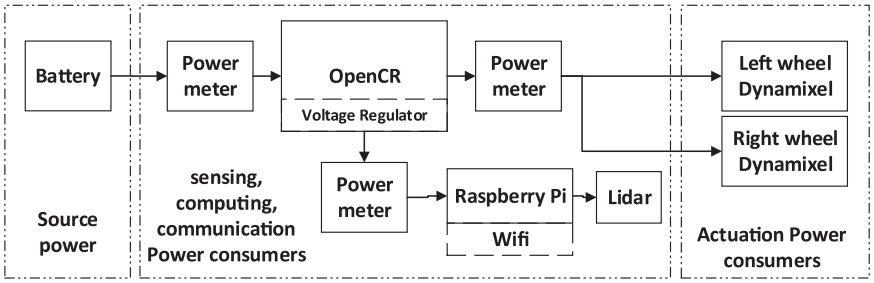

FIGURE 8 | TurtlebotBot3 (burger) power consumption breakdown for a robotic mission with a fixed configuration and setting. The whole power consumption of the robot is subdivided into actuation power and static power, including sensing, computing, and communication.

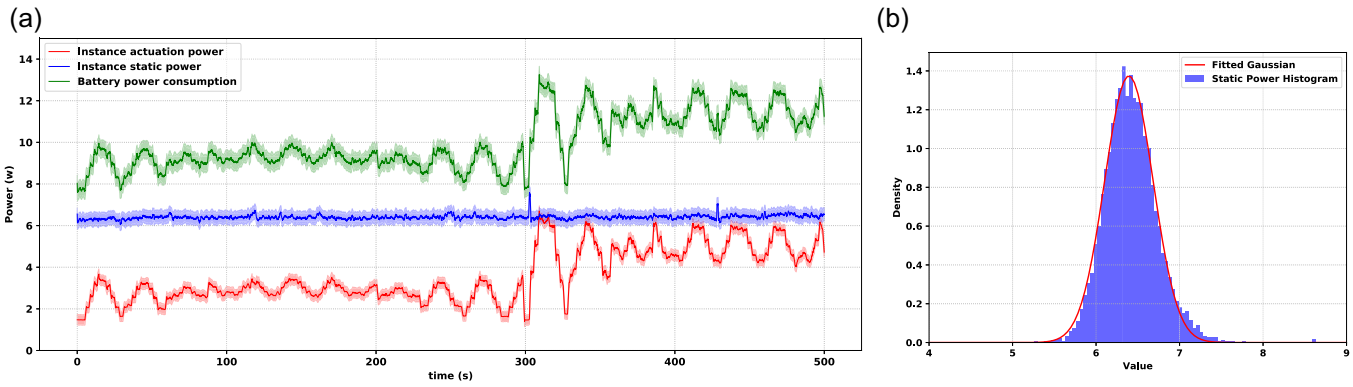

FIGURE 9 | (a) Measured instance powers of Turtlebot3 (moving averages with window size=20) with a payload change from no-load to full-load (total robot mass 1 kg→6 kg). The measurements approve the assumption that the total power consumption of the robot (green) can be subdivided into actuation power (red) and static power (blue) under certain operation conditions. (b) Histogram of measured static power consumption of the robot (blue). The estimation of the static power consumption can be represented by a fitted Gaussian distribution (red).

Section 6 and are aligned with the approach presented in this work. In the phase of offline training (step 1), we employed the measured robot's velocity and actuation power in both no-load and full-load to determine the mass-decoupled coefficients.

The wheels' velocity is computed using the linear and angular velocity of the TurtleBot odometry data (ROS topic) in combination with the robot's kinematic information. To reduce measurement noise effects in the system, the measured values are filtered through a 5th-order low-pass Butterworth filter and a uniform filter. The Z-score indicator is employed to identify outlier data in the calculated wheels' acceleration, which are then replaced with their average values. Moreover, It is crucial to ensure the accuracy of the collected data and verify that data filtering does not alter the fundamental behavior of the measurements. This guarantees that the data used for further analysis remains reliable.

Following the proposed approach, mass-decoupled coefficients are estimated using the PGD method. In contrast to the offline training phase in the simulation Section 6, different learning rates between 0.001 and 0.01 are utilized, while keeping the momentum coefficient fixed at 0.9.

Figure 10 illustrates the estimations of the robot's mass as the payload changes from 2 to 3 kg using a cumulative weighted

average with determined payload change time (see Figure 4). On the other hand, Figure 11 displays the moving average of the estimated mass with various time windows when the payload change time is undetermined, highlighting the importance of selecting the averaging period in Equation (26). Consequently, the power consumed for sensing the actuation power and computing the estimated mass varies for each of the time windows. The effects of time window choosing on the mass estimation error percentage and actuation power estimation MAPE are shown in Figure 12.

By implementing the third step of our proposed approach, the actuation power is calculated using Equation (18), estimated mass-decoupled coefficients in step one, and estimated payload in step two. Figure 13b shows the estimated output compared to the measured power in the presence of a payload change from 2 to 3 kg with a 25-s moving average time window (MATW). Prediction validation of test data for this experiment is also shown in Figure 14.

7.2 | Comparison With Other Methods

According to our literature review in Section 2, although there are a few studies investigating the power consumption estimation of GMRs with unknown payloads, none of these studies consider variable unknown payloads. To validate the proposed approach, we modified two of the recently used methods from

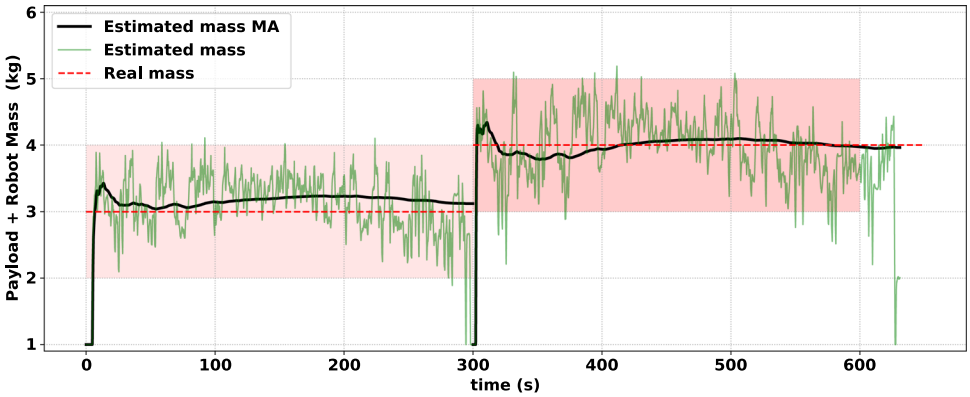

FIGURE 10 | Turtlebot3 payload estimation for the experimental data set when the payload change time is determined. The black line shows the cumulative weighted average over the estimated mass at the start of each task. The figure shows the convergence of the proposed unknown payload estimation method.

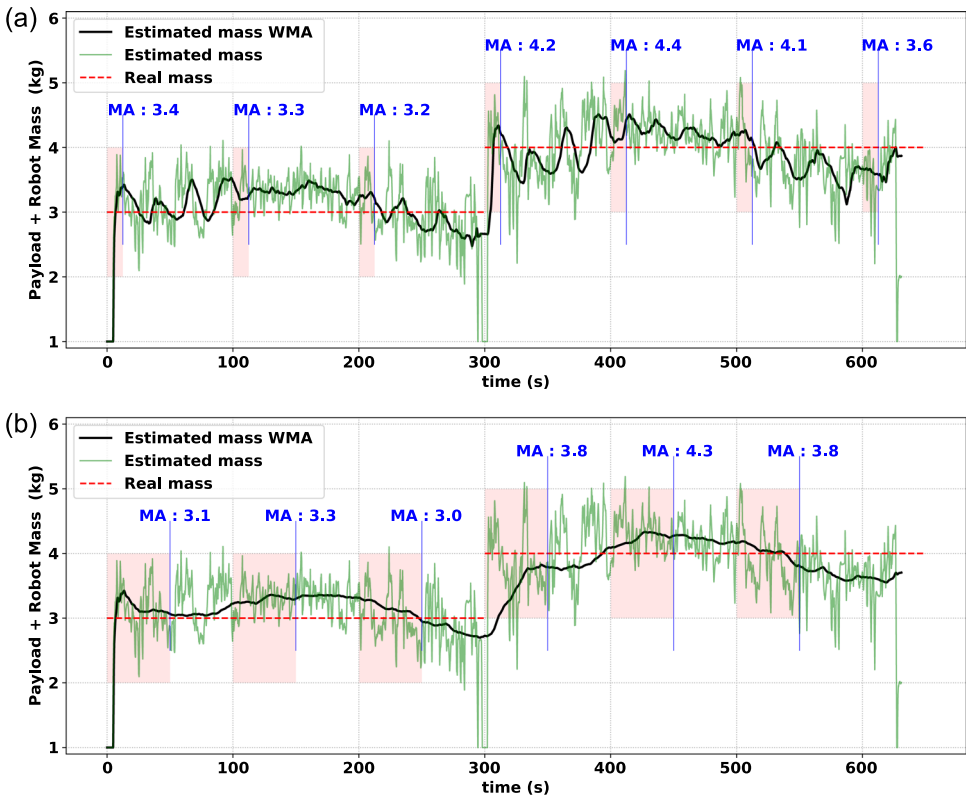

FIGURE 11 | Turtlebot3 payload estimation for the experimental data set with (a) 12.5-s, (b) 50-s time window weighted moving average (WMA) over the estimated mass. The selection of the averaging time window in the absence of payload changing time information depends on task patterns and it impacts power estimation accuracy.

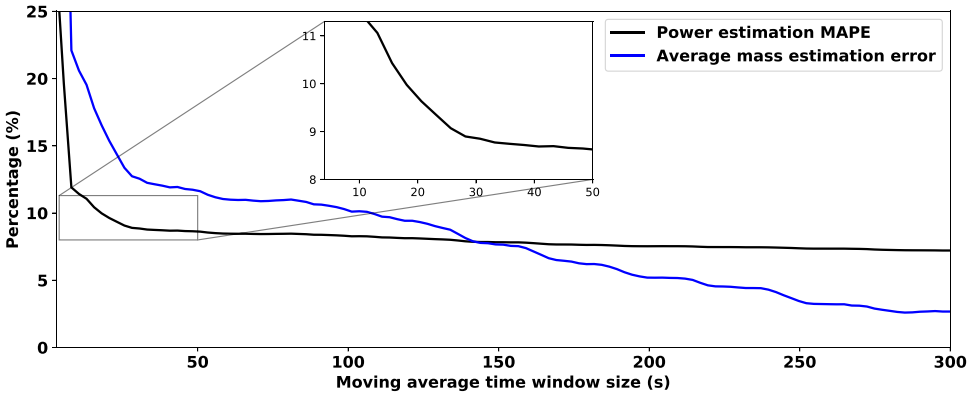

FIGURE 12 | Average percentage of mass estimation error and actuation power consumption estimation mean absolute percentage error (MAPE), selecting the worst-case time window with different moving average time window sizes for an unknown payload change. The magnified window demonstrates the minor dependency of power estimation MAPE to increased time windows higher than 30 s.

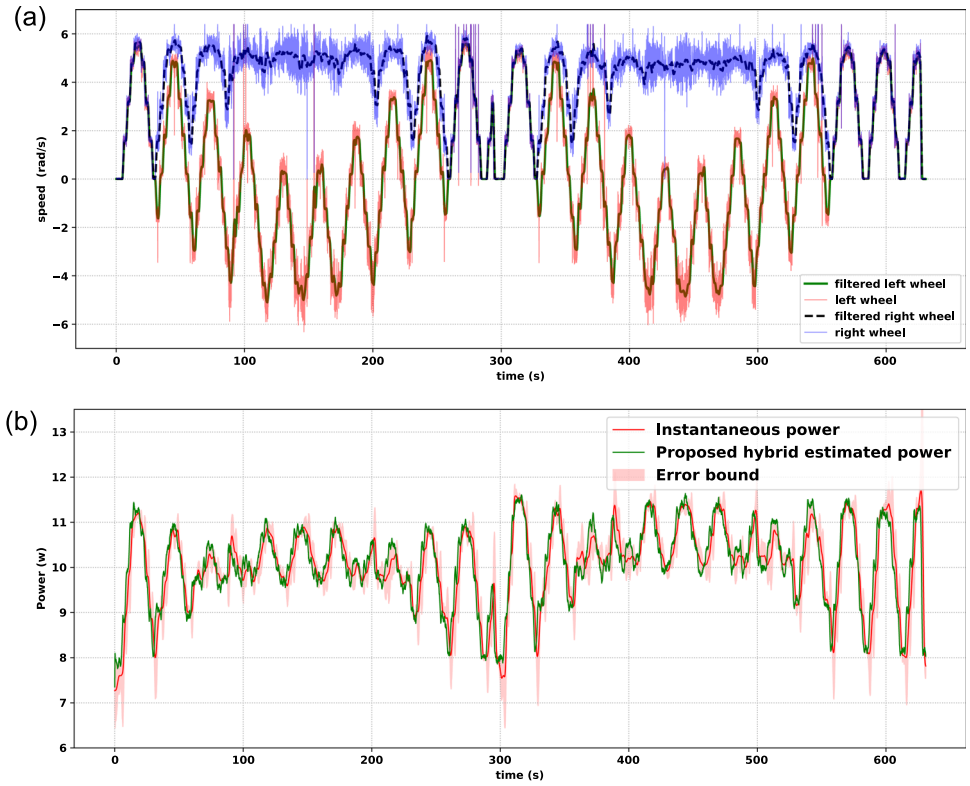

FIGURE 13 | Power estimation (b) of Turtlebot3 (Burger) for a given velocity profile (a) in the presence of payload change from 2 to 3 kg (total robot mass 3 kg→4 kg). The high noise ratio in the measurements underscores the importance of data filtering in the data processing.

Leng et al. (2024) and Liu et al. (2023) and compared these data-driven methods with our proposed method. In (Leng et al. 2024), multivariate linear regression method is used to estimate the coefficients of the following model to predict the actuation power consumption of the robot:

$$\begin{aligned} P_{act} = {} & c_0 + c_1 v + c_2 \max(\dot{v}, 0\}v + c_3 \min)\dot{v}, 0\}v \\ & + c_4 \omega + c_5 \max\{\dot{\omega}, 0\}\omega + c_6 \min\{\dot{\omega}, 0\}\omega \\ & + c_7 \max\{\sin\phi, 0\}v + c_8 \min\{\sin\phi, 0\}v \end{aligned} \tag{30}$$

where ϕ is the road grade (in radians) and can be assumed to be zero in our scenario. Although $\sin(\phi) \approx \phi$ for low road slopes ($\phi < \frac{15\pi}{180}$), which leads to combining c_7 and c_8 into c_1 when the road grade is constant in the environment. Based on the results in Parasuraman et al. (2014), Equation (30) can be further developed by adding the effect of payload mass:

$$\begin{aligned} P_{act} = {} & c_0 + c_1 v + c_2 \max(\dot{v}, 0\}v + c_3 \min)\dot{v}, 0\}v \\ & + c_4 \omega + c_5 \max\{\dot{\omega}, 0\}\omega + c_6 \min\{\dot{\omega}, 0\}\omega + c_7 m \end{aligned} \tag{31}$$

We used (31) for the first comparison method.

On the other hand, neural networks have been successfully used in recent studies for modeling the power usage of GMRs

(Góra et al. 2021; Sakayori and Ishigami 2021; Liu et al. 2023; Chikushi 2024). Specifically, Liu et al. (2023) used the control inputs and feedback from the robot's motors at different fixed speeds to train an MLP neural network, utilizing mean square error (MSE) as the loss function.

$$\min loss = \frac{1}{N}\sum_{i=1}^{N}\left(\overset{t_i}{p}_{act} - \hat{p_{act}}^{t_i}\right)^2 \quad \text{where } \hat{p_{act}}^{t} = F\left(c_0^t, ..., c_j^t, f_0^t, ..., f_j^t\right) \tag{32}$$

The trained neural network has seven hidden layers with the rectified linear unit function as the activation function for the hidden layers and a constant learning rate of 0.01. The learning process is terminated if loss or score is not improving by at least 1e−4 for 50 iterations or the number of epochs exceeds 1000.

The train and test data set for both comparing methods is kept the same as the ones used for the proposed method (payload changes from no-load to full-load for the training data set and it changes from 2 to 3 kg for the test data set). Prediction validation is compared and is shown in Figure 15.

8 | Discussion

One of our first assumptions to formulate the energy consumption in GMRs is that under consistent operating conditions and configuration of the robot, power consumption of the robot can be subdivided into static power and actuation power consumption as formulated in Equation (28). To validate this, we measured the power supplied by the robot's energy source and tracked it in its subsystems (see Figure 9a).

On the other hand, taking a different approach from most existing methods in the literature, which estimate energy consumption in GMRs assuming the weight of the robot's payload is known, our proposed method tackles the scenario where the payload is unknown during operation. To address this challenge, a hybrid parameter estimation approach is introduced for modeling the robot's actuation power. We evaluated the efficiency of the proposed method through simulation (see Figures 5 and 7) and in an experimental setting, as illustrated in Figures 13 and 14. The results demonstrate a bounded error in estimating the robot's actuation power consumption. The mean absolute percentage error of estimation is 5% in simulation and with a 10-s weighted moving average window and less than 9% in the experiment with a 50-s weighted moving average window. The high noise-to-signal ratio in the wheels' velocity measurements (see 13a), is one of the principal factors contributing to the higher error percentage in the experimental results.

Figure 6 in the simulation section illustrates the weighted moving average of the estimated mass with a 10-s time window. The figure highlights that mass estimation error is bounded and

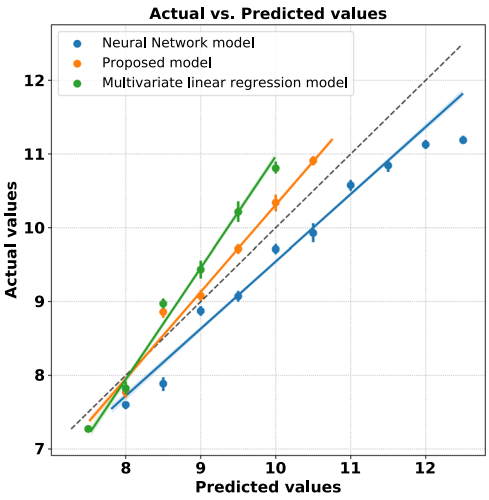

FIGURE 15 | Comparison of power consumption prediction and measured power consumption is illustrated for the proposed method with a 25-s weighted moving average (WMA) window (orange), the multi-layer perceptron (MLP) neural network model (blue), and the multivariate linear regression model (green). For clarity, power values are assigned to the nearest bin value with a 0.5-step size. The results show that the proposed method estimated actuation power consumption with better accuracy than the others across both high and low power consumption ranges.

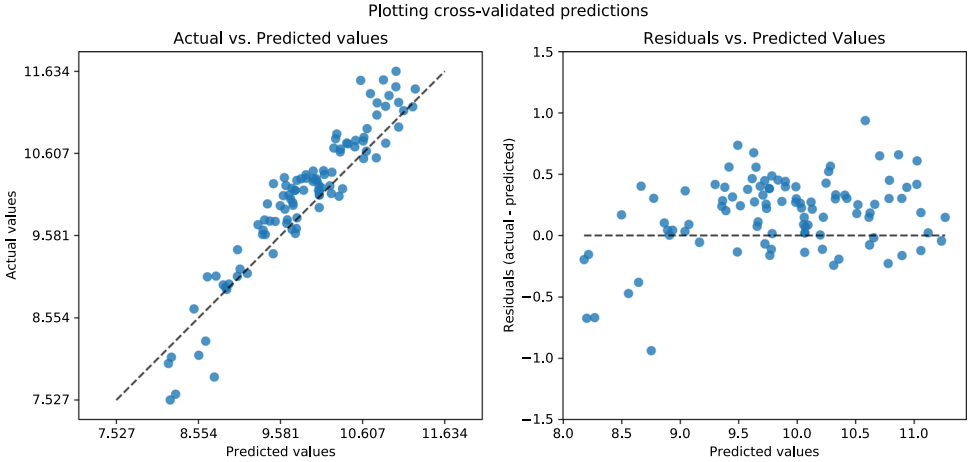

FIGURE 14 | Predictions validation of test data set in the experiment. The distribution of residuals versus predicted values (right plot) indicates the independent behavior of error to the predicted values.

depends on the time of implementing the mass estimation step. For instance, starting the mass estimation step at $t = 50$s yields an estimated mass of $\hat{m} = 4.22$ with a 5.5% error. However, performing the mass estimation with the same time window but a different starting point can result in a 22% error. Moreover, examining both Figures 6 and 5c together shows that the peak error in estimating payload occurs when the robot's wheel velocity approaches zero. In this situation, the payload estimation becomes invalid. Consequently, it is recommended to implement the second step of our proposed approach when the robot is in motion at higher speeds.

To demonstrate the advantages of the proposed method, we compared it with two different data-driven methods described in Section 7.2. In the implementation of the proposed method, a 25-s weighted moving average window was used. This approach resulted in more accurate actuation power consumption estimation, achieving a 9.12% MAPE and $R^2score = 0.78$. In comparison, the multivariate linear regression model yielded a 12.7% MAPE and an $R^2score = 0.44$ while the MLP neural network method achieved a 10.2% MAPE and $R^2score = 0.69$. In addition, Figure 15 shows the error between actual and predicted values for the implemented methods. The results show the estimation error increased for all implemented methods but variation from the baseline for the proposed approach in this study is less than the others.

Most of the dynamic models discussed in the literature focus on specific configurations of mobile robots, such as two-wheeled, four-wheeled, and others, assumed to operate in straight or predefined curved paths. In contrast, the proposed method is derived from the power consumption of various components and subsystems of the GMRs (see Figure 3), with no assumption about the path type. However, it is crucial to note that our method requires a rich data set of robot movements with different speeds and acceleration profiles to achieve accurate estimations.

Another significant aspect of the proposed solution is its adeptness in balancing estimation accuracyes and its associated costs. Figures 11 and 12 show this concept. Changing the MATW applied to the estimated mass data influences the mass estimation. A 12.5-s MATW results in an average 19.8% mass estimation error while the MAPE and R^2score of the actuation power consumption estimation are 11.1% and 0.68 when the worst-case window time is selected for conducting the second step of the proposed method. On the other hand, a 50-s MATW reduces the mass estimation error to an average of 11.6% and results in 8.6% MAPE with $R^2score = 0.79$ for the actuation power consumption estimation. The cost for this enhancement in mass estimation and actuation power consumption estimation accuracy includes the energy consumption required for measuring the essential data and the computational expenses over this additional time. The magnified section in Figure 12 shows that MATW larger than 30 s does not decrease the power consumption estimation MAPE as much as smaller MATW. This highlights the trade-off between achieving highly accurate estimations and the practical feasibility of acquiring essential data and conducting the necessary computations.

9 | Conclusion

Energy storage limitations and battery degradation present significant challenges for the efficiency, autonomy, and safety of robotic missions. This highlights the need for accurate energy consumption modeling for mobile robots. In this work, we investigated the power consumption model in GMRs with DC motors and in the context of the proposed approach, we emphasized balancing the additional sensing and computation costs with estimation accuracy over larger time windows.

In this study, we validated that under consistent conditions the power consumption of GMRs can be divided into static and actuation power consumption. In addition, unlike traditional methods that assume known payload weights, our approach addresses unknown variable payloads by using a hybrid parameter estimation model. Our simulations and experiments showed a bounded error in actuation power estimation, with a MAPE of 5% in simulations and less than 9% in experiments. Also, payload estimation errors varied from 5.5% to 22%, depending on the selected MATW for estimation. As an example, a 12.5-s MATW resulted in a 19.8% mass estimation error, while a 50-s MATW reduced the error to 11.6%. Using a 25-s MATW, our method achieved a 9.12% MAPE and an R^2score of 0.78 for actuation power consumption estimation which shows a significant performance improvement in comparison to a 12.7% MAPE and $R^2score = 0.44$ for the multivariate linear regression model and an R^2score of 0.69 with a 10.2% MAPE for the MLP neural network method.

In this work, we proposed our solution considering GMR's indoor use cases like in warehouses. For outdoor mobile robots road grade and temperature variations which are mentioned but not explored in the conducted experiments, can be incorporated into the actuation power model. Also, the proposed approach can be validated with other mobile robot platforms. Furthermore, in situations where a mobile robot can perform computations both onboard and via the cloud, determining the optimal timing and conditions for local versus cloud computing remains an unresolved question. Addressing this requires a comprehensive energy model that includes detailed submodels for both computing and communication energy consumption.

Acknowledgments

This research was supported by the IMEC, Sustainable Intelligent Sensing Project.

Conflicts of Interest

The authors declare no conflicts of interest.

Data Availability Statement

The data that support the findings of this study are available from the corresponding author upon reasonable request.

References

Ali, S. N., A. Hanif, and Q. Ahmed. 2016. "Review in Thermal Effects on the Performance of Electric Motors." In *2016 International Conference on Intelligent Systems Engineering (ICISE)*, 83–88. IEEE.

Amsters, R., and P. Slaets. 2020. “Turtlebot 3 as a Robotics Education Platform.” In *Robotics in Education: Current Research and Innovations* 10, 170–181. Springer.

Anjum, M. U., M. Khalid, and U. Manzoor. 2024. “Energy Profiling for Wheeled Mobile Robots With Lugre Friction Model in a Realistic Simulation Framework.” In *2024 IEEE International Conference on Industrial Technology (ICIT)*, 1–7. IEEE.

Bozhinoski, D., D. Di Ruscio, I. Malavolta, P. Pelliccione, and I. Crnkovic. 2019. “Safety for Mobile Robotic Systems: A Systematic Mapping Study From a Software Engineering Perspective.” *Journal of Systems and Software* 151: 150–179.

Calamai, P. H., and J. J. Moré. 1987. “Projected Gradient Methods for Linearly Constrained Problems.” *Mathematical Programming* 39, no. 1: 93–116.

Chicco, D., M. J. Warrens, and G. Jurman. 2021. “The Coefficient of Determination R-Squared is More Informative Than Smape, Mae, Mape, Mse and Rmse in Regression Analysis Evaluation.” *Peer Journal on Computer Science* 7: e623.

Chikushi, S. 2024. “A Study of Current Consumption Estimation Method for Driving System of Skid-Steering Type Mobile Robot Considering Skidding.” In *2024 IEEE/SICE International Symposium on System Integration (SII)*, 947–952. IEEE.

Dargie, W., and A. Schill. 2012. “Analysis of the Power and Hardware Resource Consumption of Servers Under Different Load Balancing Policies.” In *2012 IEEE Fifth International Conference on Cloud Computing*, 772–778. IEEE.

Datouo, R., F. B. Motto, B. E. Zobo, A. Melingui, I. Bensekrane, and R. Merzouki. 2017. “Optimal Motion Planning for Minimizing Energy Consumption of Wheeled Mobile Robots.” In *2017 IEEE International Conference on Robotics and Biomimetics (ROBIO)*, 2179–2184. IEEE.

Dogru, S., and L. Marques. 2018. “A Physics-Based Power Model for Skid-Steered Wheeled Mobile Robots.” *IEEE Transactions on Robotics* 34, no. 2: 421–433.

Effati, M., K. Skonieczny, and D. J. Balkcom. 2023. “Energy-Optimal Trajectories for Skid-Steer Rovers.” *International Journal of Robotics Research* 43, no. 2: 171–202. 02783649231216499.

Ferretti, G., G. Magnani, G. Martucci, P. Rocco, and V. Stampacchia. 2003. “Friction Model Validation in Sliding and Presliding Regimes With High Resolution Encoders.” In *Experimental Robotics* VIII, 328–337. Springer.

García, P. L., S. Crispel, E. Saerens, T. Verstraten, and D. Lefeber. 2020. “Compact Gearboxes for Modern Robotics: A Review.” *Frontiers in Robotics and AI* 7: 103.

Garcia, P. L., S. Crispel, A. Varadharajan, et al. 2022. “R2power: The Proof-of-Concept of a Backdrivable, High-Ratio Gearbox for Human-Robot Collaboration.” In *2022 International Conference on Robotics and Automation (ICRA)*, 1–7. IEEE.

Goldstein, A. A. 1964. “Convex Programming in Hilbert Space.” *Bulletin of the American Mathematical Society* 70: 709–710.

Góra, K., M. Kujawinski, D. Wroński, and G. Granosik. 2021. “Comparison of Energy Prediction Algorithms for Differential and Skid-Steer Drive Mobile Robots on Different Ground Surfaces.” *Energies* 14, no. 20: 6722.

Gürgöze, G., and İ. Türkoğlu. 2022. “A Novel Energy Consumption Model for Autonomous Mobile Robot.” *Turkish Journal of Electrical Engineering and Computer Sciences* 30, no. 1: 216–232.

Han, X., L. Lu, Y. Zheng, et al. 2019. “A Review on the Key Issues of the Lithium Ion Battery Degradation Among the Whole Life Cycle.” *ETransportation* 1: 100005.

Hou, L., L. Zhang, and J. Kim. 2018. “Energy Modeling and Power Measurement for Mobile Robots.” *Energies* 12, no. 1: 27.

Hou, L., F. Zhou, K. Kim, and L. Zhang. 2021. “Practical Model for Energy Consumption Analysis of Omnidirectional Mobile Robot.” *Sensors* 21, no. 5: 1800.

INA219 Zero-Drift.2015. *Zero-Drift, Bidirectional Current/Power Monitor With I2C Interface*. Texas Instruments Inc.

Jaiem, L., D. Crestani, L. Lapierre, and S. Druon. 2021. “Energy Consumption of Control Schemes for the Pioneer 3dx Mobile Robot: Models and Evaluation.” *Journal of Intelligent & Robotic Systems* 102, no. 1: 23.

Jaiem, L., S. Druon, L. Lapierre, and D. Crestani. 2016. “A Step Toward Mobile Robots Autonomy: Energy Estimation Models.” In *Towards Autonomous Robotic Systems: 17th Annual Conference, TAROS 2016, Sheffield, UK, June 26–July 1, 2016, Proceedings* 17, 177–188. Springer.

Jaramillo-Morales, M. F., S. Dogru, J. B. Gomez-Mendoza, and L. Marques. 2020. “Energy Estimation for Differential Drive Mobile Robots on Straight and Rotational Trajectories.” *International Journal of Advanced Robotic Systems* 17, no. 2: 1729881420909654.

Jaramillo-Morales, M. F., S. Dogru, L. Marques, and J. B. Gomez-Mendoza. 2019. “Predictive Power Estimation for a Differential Drive Mobile Robot Based on Motor and Robot Dynamic Models.” In *2019 Third IEEE International Conference on Robotic Computing (IRC)*, 301–307. IEEE.

Kim, H., and B. K. Kim. 2012. “Minimum-Energy Trajectory Planning and Control on a Straight Line With Rotation for Three-Wheeled Omni-Directional Mobile Robots.” In *2012 IEEE/RSJ International Conference on Intelligent Robots and Systems*, 3119–3124. IEEE.

Kim, H., and B. K. Kim. 2017. “Minimum-Energy Cornering Trajectory Planning With Self-Rotation for Three-Wheeled Omni-Directional Mobile Robots.” *International Journal of Control, Automation and Systems* 15: 1857–1866.

Kumar, P., I. Bensekrane, and R. Merzouki. 2022. “Power Consumption Modeling of Wheeled Mobile Robots With Multiple Driving Modes.” In *IEEE Transactions on Industrial Electronics*. IEEE.

Leng, J., J. Peng, J. Liu, Y. Zhang, J. Ji, and Y. Zhang. 2024. “Profiling Power Consumption in Low-Speed Autonomous Guided Vehicles.” In *IEEE Robotics and Automation Letters*. IEEE.

Liang, D., F. Ma, and W. Li. 2020. “New Gradient-Weighted Adaptive Gradient Methods With Dynamic Constraints.” *IEEE Access* 8: 110929–110942.

Licea, D. B., M. Ghogho, and M. Saska. 2024. “When Robotics Meets Wireless Communications: An Introductory Tutorial.” In *Proceedings of the IEEE*. IEEE.

Liu, L., R. Zhong, A. Willcock, N. Fisher, and W. Shi. 2023. “An Open Approach to Energy-Efficient Autonomous Mobile Robots.” In *2023 IEEE International Conference on Robotics and Automation (ICRA)*, 11569–11575. IEEE.

Mei, Y., Y.-H. Lu, Y. C. Hu, and C. G. Lee. 2005. “A Case Study of Mobile Robot's Energy Consumption and Conservation Techniques.” In *ICAR'05. Proceedings of the 12th International Conference on Advanced Robotics*, 492–497. IEEE.

Merkel, A., J. Stoess, and F. Bellosa. 2010. “Resource-Conscious Scheduling for Energy Efficiency on Multicore Processors.” In *Proceedings of the 5th European Conference on Computer Systems*, 153–166.

Mikołajczyk, T., D. Mikołajewski, A. Kłodowski, et al. 2023. “Energy Sources of Mobile Robot Power Systems: A Systematic Review and Comparison of Efficiency.” *Applied Sciences* 13, no. 13: 7547.

Mohammadpour, M., L. Zeghmi, S. Kelouwani, M.-A. Gaudreau, A. Amamou, and M. Graba. 2021. “An Investigation Into the Energy-Efficient Motion of Autonomous Wheeled Mobile Robots.” *Energies* 14, no. 12: 3517.

Morales, M. F. J., and J. B. G. Mendoza. 2018. “Mixed Energy Model for a Differential Guide Mobile Robot.” In *2018 23rd International*

Conference on Methods & Models in Automation & Robotics (MMAR), 114–119. IEEE.

Parasuraman, R., K. Kershaw, P. Pagala, and M. Ferre. 2014. "Model Based On-line Energy Prediction System for Semi-Autonomous Mobile Robots." In *2014 5th International Conference on Intelligent Systems, Modelling and Simulation*, 411–416. IEEE.

Parasuraman, R., P. Pagala, K. Kershaw, and M. Ferre. 2012. "Energy Management Module for Mobile Robots in Hostile Environments." In *Advances in Autonomous Robotics: Joint Proceedings of the 13th Annual TAROS Conference and the 15th Annual FIRA RoboWorld Congress, Bristol, UK, August 20–23, 2012*, 13, 430–431. Springer.

Pentzer, J., S. Brennan, and K. Reichard. 2022. "On-Line Estimation of Power Model Parameters for Skid-Steer Robots With Applications in Mission Energy Use Prediction." *Journal of Field Robotics* 39, no. 6: 763–782.

Quann, M., L. Ojeda, W. Smith, D. Rizzo, M. Castanier, and K. Barton. 2020. "Off-Road Ground Robot Path Energy Cost Prediction Through Probabilistic Spatial Mapping." *Journal of Field Robotics* 37, no. 3: 421–439.

Reddi, S. J., S. Kale, and S. Kumar. 2019. " On the Convergence of Adam and Beyond." arXiv preprint arXiv:1904.09237.

Sadrpour, A., J. Jin, and A. G. Ulsoy. 2012. "Mission Energy Prediction for Unmanned Ground Vehicles." In *2012 IEEE International Conference on Robotics and Automation*, 2229–2234. IEEE.

Sadrpour, A., J. Jin, and A. G. Ulsoy. 2013a. "Experimental Validation of Mission Energy Prediction Model for Unmanned Ground Vehicles." In *2013 American Control Conference*, 5960–5965. IEEE.

Sadrpour, A., J. Jin, and A. G. Ulsoy. 2013b. "Mission Energy Prediction for Unmanned Ground Vehicles Using Real-Time Measurements and Prior Knowledge." *Journal of Field Robotics* 30, no. 3: 399–414.

Sakayori, G., and G. Ishigami. 2021. "Energy-Aware Trajectory Planning for Planetary Rovers." *Advanced Robotics* 35, no. 21–22: 1302–1316.

Siwek, M., J. Panasiuk, L. Baranowski, W. Kaczmarek, P. Prusaczyk, and S. Borys. 2023. "Identification of Differential Drive Robot Dynamic Model Parameters." *Materials* 16, no. 2: 683.

Srikantaiah, S., A. Kansal, and F. Zhao. 2008. "Energy Aware Consolidation for Cloud Computing." In *USENIX HotPower'08: Workshop on Power Aware Computing and Systems at OSDI*, 1–5.

Touzout, W., D. Benazzouz, and Y. Benmoussa. 2022. "Mobile Robot Energy Modelling Integrated Into ROS and Gazebo-Based Simulation Environment." *Mechatronic Systems and Control (formerly Control and Intelligent Systems)* 50, no. 2: 66–73.

Unger, H., T. Markert, and E. Müller. 2018. "Evaluation of Use Cases of Autonomous Mobile Robots in Factory Environments." *Procedia Manufacturing* 17: 254–261.

Verstraten, T. 2018. "New Actuation Paradigms With High Efficiency For Variable Load At Varying Speed." PhD thesis, Vrije Universiteit Brussel Belgium, Brussel.

Verstraten, T., R. Furnémont, G. Mathijssen, B. Vanderborght, and D. Lefeber. 2016. "Energy Consumption of Geared Dc Motors in Dynamic Applications: Comparing Modeling Approaches." *IEEE Robotics and Automation Letters* 1, no. 1: 524–530.

Verstraten, T., M. S. Hosen, M. Berecibar, and B. Vanderborght. 2023. "Selecting Suitable Battery Technologies for Untethered Robot." *Energies* 16, no. 13: 4904.

Wahab, M., F. Rios-Gutierrez, and A. El Shahat. 2015. *Energy Modeling of Differential Drive Robots*. IEEE.

Wang, J., Y. Song, F. Liu, and R. Hou. 2016. "Analysis and Application of Forecasting Models in Wind Power Integration: A Review of Multi-Step-Ahead Wind Speed Forecasting Models." *Renewable and Sustainable Energy Reviews* 60: 960–981.

Yacoub, M. I., D. S. Necsulescu, and J. Z. Sasiadek. 2013. "Experimental Evaluation of Energy Optimization Algorithm for Mobile Robots in Three-Dimension Motion Using Predictive Control." In *21St Mediterranean Conference on Control and Automation*, 437–443. IEEE.

Yao, M., H. Deng, X. Feng, P. Li, Y. Li, and H. Liu. 2024. "Improved Dynamic Windows Approach Based on Energy Consumption Management and Fuzzy Logic Control for Local Path Planning of Mobile Robots." *Computers & Industrial Engineering* 187: 109767.

Zhang, H., Y. Zhang, and T. Yang. 2020. "A Survey of Energy-Efficient Motion Planning for Wheeled Mobile Robots." *Industrial Robot: The International Journal of Robotics Research and Application* 47, no. 4: 607–621.

Zhou, Z., W. Tang, M. Li, W. Cao, and Z. Yuan. 2023. "A Novel Hybrid Intelligent Sopdel Model With Comprehensive Data Preprocessing for Long-Time-Series Climate Prediction." *Remote Sensing* 15, no. 7: 1951.

Zorbas, D., and T. Razafindralambo. 2015. " Modeling the Power Consumption of a Wifibot and Studying the Role of Communication Cost in Operation Time." arXiv preprint arXiv:1512.04380.